ACCOUNTS
of chemical research

Theory of Chemical Kinetics and Charge Transfer based on Nonequilibrium Thermodynamics

MARTIN Z. BAZANT*

Departments of Chemical Engineering and Mathematics, Massachusetts Institute of Technology, Cambridge, Massachusetts 02139, United States

RECEIVED ON JULY 20, 2012

CONSPECTUS

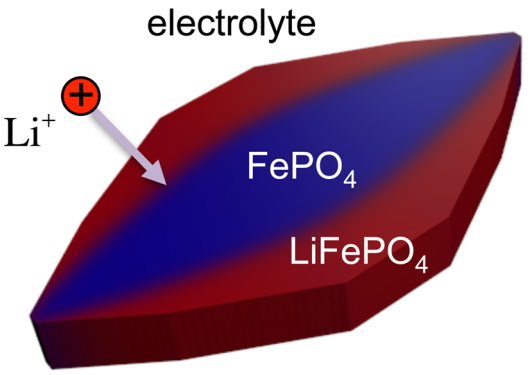

Advances in the fields of catalysis and electrochemical energy conversion often involve nanoparticles, which can have kinetics surprisingly different from the bulk material. Classical theories of chemical kinetics assume independent reactions in dilute solutions, whose rates are determined by mean concentrations. In condensed matter, strong interactions alter chemical activities and create variations that can dramatically affect the reaction rate. The extreme case is that of a reaction coupled to a phase transformation, whose kinetics must depend not only on the order parameter but also on its gradients at phase boundaries. Reaction-driven phase transformations are common in electrochemistry, when charge transfer is accompanied by ion intercalation or deposition in a solid phase. Examples abound in Li-ion, metal–air, and lead–acid batteries, as well as metal electrodeposition–dissolution. Despite complex thermodynamics, however, the standard kinetic model is the Butler–Volmer equation, based on a dilute solution approximation. The Marcus theory of charge transfer likewise considers isolated reactants and neglects elastic stress, configurational entropy, and other nonidealities in condensed phases.

The limitations of existing theories recently became apparent for the Li-ion battery material Li_xFePO_4 (LFP). It has a strong tendency to separate into Li-rich and Li-poor solid phases, which scientists believe limits its performance. Chemists first modeled phase separation in LFP as an isotropic "shrinking core" within each particle, but experiments later revealed striped phase boundaries on the active crystal facet. This raised the question: What is the reaction rate at a surface undergoing a phase transformation? Meanwhile, dramatic rate enhancement was attained with LFP nanoparticles, and classical battery models could not predict the roles of phase separation and surface modification.

In this Account, I present a general theory of chemical kinetics, developed over the past 7 years, which is capable of answering these questions. The reaction rate is a nonlinear function of the thermodynamic driving force, the free energy of reaction, expressed in terms of variational chemical potentials. The theory unifies and extends the Cahn–Hilliard and Allen–Cahn equations through a master equation for nonequilibrium chemical thermodynamics. For electrochemistry, I have also generalized both Marcus and Butler–Volmer kinetics for concentrated solutions and ionic solids.

This new theory provides a quantitative description of LFP phase behavior. Concentration gradients and elastic coherency strain enhance the intercalation rate. At low currents, the charge-transfer rate is focused on exposed phase boundaries, which propagate as "intercalation waves", nucleated by surface wetting. Unexpectedly, homogeneous reactions are favored above a critical current and below a critical size, which helps to explain the rate capability of LFP nanoparticles. Contrary to other mechanisms, elevated temperatures and currents may enhance battery performance and lifetime by suppressing phase separation. The theory has also been extended to porous electrodes and could be used for battery engineering with multiphase active materials.

More broadly, the theory describes nonequilibrium chemical systems at mesoscopic length and time scales, beyond the reach of molecular simulations and bulk continuum models. The reaction rate is consistently defined for inhomogeneous, nonequilibrium states, for example, with phase separation, large electric fields, or mechanical stresses. This research is also potentially applicable to fluid extraction from nanoporous solids, pattern formation in electrophoretic deposition, and electrochemical dynamics in biological cells.

Published on the Web 03/22/2013 www.pubs.acs.org/accounts
10.1021/ar300145c

Introduction

Breakthroughs in catalysis and electrochemical energy conversion often involve nanoparticles, whose kinetics can differ unexpectedly from the bulk material. Perhaps the most remarkable case is lithium iron phosphate, Li_xFePO_4 (LFP). In the seminal study of micrometer-sized LFP particles, Padhi et al.[1] concluded that "the material is very good for low-power applications" but "at higher current densities there is a reversible decrease in capacity that... is associated with the movement of a two-phase interface" between $LiFePO_4$ and $FePO_4$. Ironically, over the next decade, in nanoparticle form, LFP became the most popular high-power cathode material for Li-ion batteries.[2−4] Explaining this reversal of fortune turned out to be a major scientific challenge, with important technological implications.

It is now understood that phase separation is strongly suppressed in LFP nanoparticles, to some extent in equilibrium[5−8] but especially under applied current,[7,9−11] since reaction limitation,[12] anisotropic lithium transport,[13−16] elastic coherency strain,[7,17−19] and interfacial energies[8,9,20,21] are all enhanced. At low currents, anisotropic nucleation and growth can also occur,[7−9,12,22] as well as multiparticle mosaic instabilities.[23−26] These complex phenomena cannot be described by traditional battery models,[27,28] which assume a spherical "shrinking core" phase boundary.[29,30]

This Account summarizes my struggle to develop a phase-field theory of electrochemical kinetics[6−9,12,19,26,33−35] by combining charge-transfer theory[36] with concepts from statistical physics[37] and nonequilibrium thermodynamics.[38−40] It all began in 2006 when my postdoctoral associate, Gogi Singh, found the paper of Chen et al.[31] revealing striped phase boundaries in LFP, looking nothing like a shrinking core and suggesting phase boundary motion perpendicular to the lithium flux (Figure 1). It occurred to me that, at such a surface, intercalation reactions must be favored on the phase boundary in order to preserve the stable phases, but this could not be described by classical kinetics proportional to concentrations. Somehow the reaction rate had to be sensitive to concentration gradients.

As luck would have it, I was working on models of charge relaxation in concentrated electrolytes using nonequilibrium thermodynamics,[35,41] and this seemed like a natural starting point. Gerbrand Ceder suggested adapting the Cahn−Hilliard (CH) model for LFP,[42] but it took several years to achieve a consistent theory. Our initial manuscript[43] was rejected in 2007, just after Gogi left MIT and I went on sabbatical leave to ESPCI, faced with rewriting the paper.[12]

The rejection was a blessing in disguise, since it made me think harder about the foundations of chemical kinetics. The paper contained some new ideas, phase-field chemical kinetics and intercalation waves, that, the reviewers felt, contradicted the laws of electrochemistry. It turns out the basic concepts were correct, but Ken Sekimoto and David Lacoste at ESPCI helped me realize that my initial Cahn−Hilliard reaction (CHR) model did not uphold the De Donder relation.[37] In 2008 in Paris, I completed the theory, prepared lecture notes,[33] published generalized Butler−Volmer kinetics[35] (section 5.4.2) and formulated nonequilibrium thermodynamics for porous electrodes[26] (see also Sekimoto[37]).

Phase-field kinetics represents a paradigm shift in chemical physics, which my group has successfully applied to Li-ion batteries. Damian Burch[6] used the CHR model to study intercalation in nanoparticles, and his thesis[25] included early simulations of "mosaic instability" in collections of bistable particles.[23,24] Simulations of galvanostatic discharge by Peng Bai and Daniel Cogswell led to the unexpected prediction of a critical current for the suppression of phase separation.[9] Liam Stanton modeled anisotropic coherency strain,[19] which Dan added to our LFP model,[7] along with

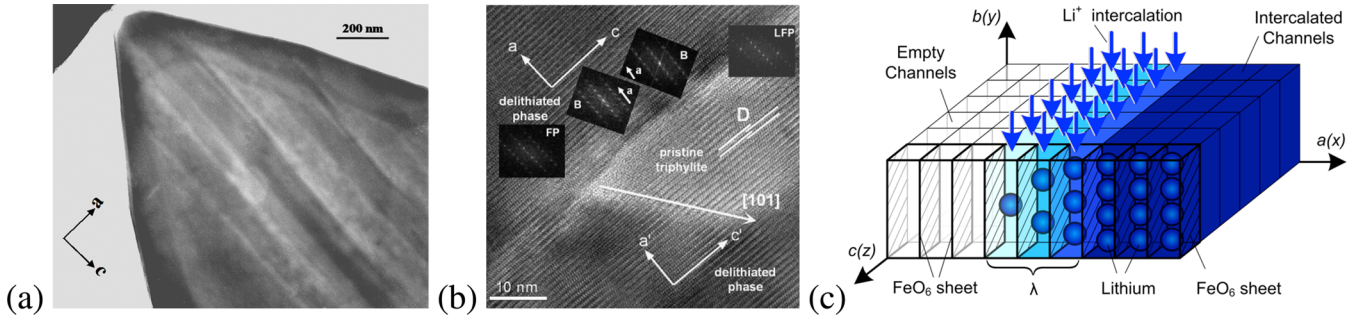

FIGURE 1. Motivation to generalize charge-transfer theory. Observations by (a) Chen et al.[31] and (b) Ramana et al.[32] of separated $FePO_4$ and $LiFePO_4$ phases on the active {010} facet, which suggest (c) focusing of lithium intercalation reactions on the phase boundary, so it propagates as an "intercalation wave"[12] (or "domino cascade"[15]). From refs 12, 31, and 32.

surface wetting.[8] Using material properties from *ab initio* calculations, Dan predicted phase behavior in LFP[7] and the critical voltage for nucleation[8] in excellent agreement with experiments. Meanwhile, Todd Ferguson[26] did the first simulations of phase separation in porous electrodes, paving the way for engineering applications.

What follows is a general synthesis of the theory and a summary of its key predictions. A thermodynamic framework is developed for chemical kinetics, whose application to charge transfer generalizes the classical Butler–Volmer and Marcus equations. The theory is then unified with phase-field models and applied to Li-ion batteries.

Reactions in Concentrated Solutions

Generalized Kinetics. The theory is based on chemical thermodynamics. In an open system, the chemical potential of species *i* (per particle),

$$\mu_i = k_B T \ln a_i + \mu_i^\ominus = k_B T \ln \tilde{c}_i + \mu_i^{ex} \quad (1)$$

is defined relative to a standard state ($\ominus$) of unit activity ($a_i = 1$) and concentration $c_i = c_i^\ominus$, where $\tilde{c}_i = c_i/c_i^\ominus$ is the dimensionless concentration. The activity coefficient,

$$\gamma_i = e^{(\mu_i^{ex} - \mu_i^\ominus)/(k_B T)} \quad (2)$$

is a measure of nonideality ($a_i = \gamma_i \tilde{c}_i$). In a dilute solution, $\mu_i^{ex} = \mu_i^\ominus$ and $\gamma_i = 1$. For the general chemical reaction,

$$S_1 = \sum_r s_r A_r \rightarrow \sum_p s_p B_p = S_2 \quad (3)$$

the equilibrium constant is

$$K^\ominus = \left(\frac{a_2}{a_1}\right)^{eq} = e^{(\mu_1^\ominus - \mu_2^\ominus)/(k_B T)} \quad (4)$$

where $a_1 = \prod_r a_r^{s_r}$, $a_2 = \prod_p a_p^{s_p}$, $\mu_1^\ominus = \sum_r s_r \mu_r^\ominus$ and $\mu_2^\ominus = \sum_p s_p \mu_p^\ominus$.

The theory assumes that departures from equilibrium obey linear irreversible thermodynamics (LIT).[38,39] The flux of species *i* is proportional to the thermodynamic driving force, $-\nabla\mu_i$:

$$F_i = -M_i c_i \nabla\mu_i = -D_i\left(\nabla c_i + c_i \nabla \frac{\mu_i^{ex}}{k_B T}\right) = -D_i^{chem} \nabla c_i \quad (5)$$

where M_i is the mobility, $D_i = M_i k_B T$ is the tracer diffusivity, and $D_i^{chem} = D_i(1 + (\partial \ln \gamma_i)/(\partial \ln c_i))$ is the chemical diffusivity.[28] In eq 5, the first term represents random fluctuations and the second drift in response to the thermodynamic bias, $-\nabla\mu_i^{ex}$.

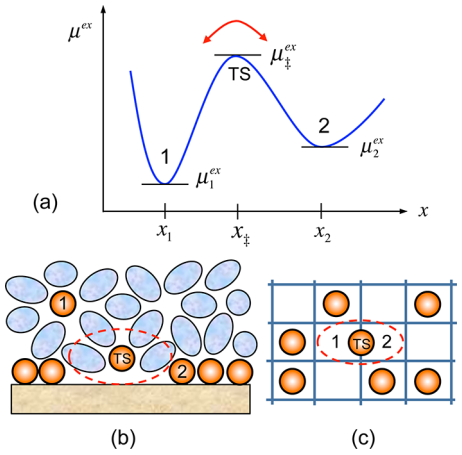

FIGURE 2. (a) Landscape of excess chemical potential explored by the reaction $S_1 \rightarrow S_2$. (b) Adsorption from a liquid, where the transition state (TS) excludes multiple surface sites ($s > 1$) while shedding the first-neighbor shell. (c) Solid diffusion on a lattice, where the transition state excludes two sites.

In a consistent formulation of reaction kinetics,[33,37] therefore, the reaction complex explores a landscape of excess chemical potential, $\mu^{ex}(x)$ between local minima μ_1^{ex} and μ_2^{ex} with transitions over an activation barrier μ^{ex} (Figure 2a). For rare transitions ($\mu_\ddagger^{ex} - \mu_{1,2}^{ex} \gg k_B T$), the reaction rate (per site) is

$$R = k_\rightarrow \tilde{c}_1 e^{-(\mu_\ddagger^{ex} - \mu_1^{ex})/(k_B T)} - k_\leftarrow \tilde{c}_2 e^{-(\mu_\ddagger^{ex} - \mu_2^{ex})/(k_B T)} \quad (6)$$

Enforcing detailed balance ($R = 0$) in equilibrium ($\mu_1 = \mu_2$) yields the reaction rate consistent with nonequilibrium thermodynamics:

$$R = k_0 (e^{-(\mu_\ddagger^{ex} - \mu_1)/(k_B T)} - e^{-(\mu_\ddagger^{ex} - \mu_2)/(k_B T)}) \quad (7)$$

where $k_0 = k_\rightarrow = k_\leftarrow$ (for properly defined μ). Equation 7 upholds the De Donder relation,[37]

$$\frac{R_\rightarrow}{R_\leftarrow} = \frac{K^\ominus a_1}{a_2} = e^{(\mu_1 - \mu_2)/(k_B T)} \quad (8)$$

which describes the steady state of chemical reactions in open systems.[44]

The thermodynamic driving force is

$$\Delta\mu = \mu_2 - \mu_1 = k_B T \ln \frac{a_2}{K^\ominus a_1} = \Delta G \quad (9)$$

also denoted as ΔG, the free energy of reaction. The reaction rate eq 7 can be expressed as a nonlinear function of $\Delta\mu$:

$$R = R_0(e^{-\alpha\Delta\mu/(k_BT)} - e^{(1-\alpha)\Delta\mu/(k_BT)}) \quad (10)$$

where α, the symmetry factor or generalized Brønsted coefficient,[36] is approximately constant with $0 < \alpha < 1$ for many reactions. Defining the activity coefficient of the transition state, $\gamma_\ddagger$, by

$$\mu_\ddagger^{ex} = k_BT \ln \gamma_\ddagger + (1-\alpha)\mu_1^\ominus + \alpha\mu_2^\ominus \quad (11)$$

the exchange rate R_0 takes the form

$$R_0 = \frac{k_0 a_1^{1-\alpha} a_2^{\alpha}}{\gamma_\ddagger} = k_0 \tilde{c}_1^{1-\alpha}\tilde{c}_2^{\alpha}\left(\frac{\gamma_1^{1-\alpha}\gamma_2^{\alpha}}{\gamma_\ddagger}\right) \quad (12)$$

where the term in parentheses is the thermodynamic correction for a concentrated solution.

Example: Surface Adsorption. Let us apply the formalism to Langmuir adsorption, $A \rightarrow A_{ads}$, from a liquid mixture with $\mu_1 = k_BT \ln a$ (Figure 2b). The surface is an ideal solution of adatoms and vacancies,

$$\mu_2 = k_BT \ln \frac{\tilde{c}}{1-\tilde{c}} + E_{ads} \quad (13)$$

with coverage $\tilde{c} = c/c_s$, site density c_s, and adsorption energy $E_{ads} = \mu_2^\ominus - \mu_1^\ominus$. Equilibrium yields the Langmuir isotherm,

$$\tilde{c}_{eq} = \frac{K^\ominus a}{1+K^\ominus a}, \quad K^\ominus = e^{-E_{ads}/(k_BT)} \quad (14)$$

If the transition state excludes s surface sites,

$$\mu_\ddagger^{ex} = -sk_BT \ln(1-\tilde{c}) + E_\ddagger \quad (15)$$

then eq 7 yields

$$R = k_1(1-\tilde{c})^{s-1}[K^\ominus a(1-\tilde{c}) - \tilde{c}] \quad (16)$$

where $k_1 = k_0\, e^{(E_{ads}-E_\ddagger)/(k_BT)}$ and $E_\ddagger$ is the transition state energy relative to the bulk. With only configurational entropy, we recover standard kinetics of adsorption, $A_{sol} + sV \rightarrow A_{surf} + (s-1)V$, involving s vacancies. With attractive forces, however, eq 7 predicts novel kinetics for inhomogeneous surfaces undergoing condensation (below).

Example: Solid Diffusion. We can also derive the LIT flux, eq 5, for macroscopic transport in a solid by activated hopping between adjacent minima of μ^{ex} having slowly varying chemical potential, $|\Delta\mu| \ll k_BT$ and concentration $\Delta\tilde{c} \ll 1$. Linearizing the hopping rate,

$$R \approx -\frac{R_0\Delta\mu}{k_BT}, \quad R_0 \approx \frac{k_0\tilde{c}\gamma}{\gamma_\ddagger} \quad (17)$$

over a distance Δx through an area $\Delta y\Delta z$ with $\partial\mu/\partial x \approx \Delta\mu/\Delta x$, we obtain eq 5 with

$$\frac{D}{D_0} = \frac{\gamma}{\gamma_\ddagger} \quad (18)$$

where $D_0 = k_0\Delta x/(c^\ominus\Delta y\Delta z)$. Equation 18 can be used to derive the tracer diffusivity in a concentrated solid solution by estimating $\gamma_\ddagger$ consistent with γ. For example, for diffusion on a lattice (Figure 2c) with $\gamma = (1-\tilde{c})^{-1}$, the transition state excludes two sites, $\gamma_\ddagger = (1-\tilde{c})^{-2}$; the tracer diffusivity, $D = D_0(1-\tilde{c})$, scales with the mean number of empty neighboring sites, but the chemical diffusivity is constant, $D^{chem} = D_0 = D(0)$ (particle/hole duality).

Electrochemistry in Concentrated Solutions

Electrochemical Thermodynamics. Next we apply eq 7 to the general Faradaic reaction,

$$S_1 = \sum_i s_{i,O} O_i^{z_{j,O}} + ne^- \rightarrow \sum_j s_{j,R} R_j^{z_{j,R}} = S_2 \quad (19)$$

converting the oxidized state $O^{z_O} = \sum_i s_{i,O} O_i^{z_{i,O}}$ to the reduced state $R^{z_R} = \sum_j s_{j,R} R_j^{z_{j,R}}$ while consuming n electrons. Let $\mu_1 = \mu_O + n\mu_e = \sum_i s_{i,O}\mu_{i,O} + n\mu_e$ and $\mu_2 = \mu_R = \sum_j s_{j,R}\mu_{j,R}$. Charge conservation implies $z_O - n = z_R$ where $z_O = \sum_i s_{i,O} z_{i,O}$ and $z_R = \sum_j s_{j,R} z_{j,R}$. The electrostatic energy, $z_i e\phi_i$, is added to μ_i^{ex} to define the electrochemical potential,

$$\mu_i = k_BT \ln a_i + \mu_i^\ominus + z_i e\phi_i = k_BT \ln \tilde{c}_i + \mu_i^{ex} \quad (20)$$

where $z_i e$ is the charge and ϕ_i is the Coulomb potential of mean force.

The electrostatic potential is ϕ_e in the electrode and ϕ in the electrolyte. The difference is the interfacial voltage, $\Delta\phi = \phi_e - \phi$. The mean electric field $-\nabla\phi$ at a point is unique, so $\phi_i = \phi_e$ for ions in the electrode and $\phi_i = \phi$ for those in the electrolyte solution. In the most general case of a mixed ion-electron conductor, the reduced and oxidized states are split across the interface (Figure 3a). Charge conservation implies $z_{Oe} + z_{Os} - n = z_{Re} + z_{Rs}$, and the net charge $n_c e$ transferred from the solution to the electrode is given by $n_c = z_{Os} - z_{Rs} = z_{Re} - z_{Oe} + n$.

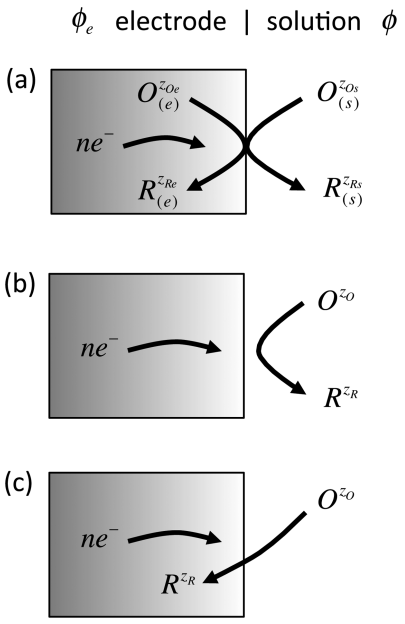

FIGURE 3. Types of Faradaic reactions $O + ne^- \rightarrow R$. (a) General mixed ion-electron conductor electrode/electrolyte interface. (b) Redox in solution. (c) Ion intercalation or electrodeposition.

Let us assume that ions only exist in the electrolyte ($z_{Re} = z_{Oe} = 0$, $n_c = n$) since the extension to mixed ion-electron conductors is straightforward. For redox reactions (Figure 3b), for example, $Fe^{3+} + e^- \rightarrow Fe^{2+}$, the reduced state is in the solution at the same potential, $\phi_R = \phi_O = \phi$. For electrodeposition (Figure 3c), for example, $Cu^{2+} + 2e^- \rightarrow Cu$, or ion intercalation as a neutral polaron, for example, $CoO_2 + Li^+ + e^- \rightarrow LiCoO_2$, the reduced state is uncharged, $z_R = 0$, so we can also set $\phi_R = \phi$, even though it is in the electrode. For this broad class of Faradaic reactions, we have

$$\mu_O = k_B T \ln a_O + \mu_O^\ominus + z_O e\phi \tag{21}$$

$$\mu_R = k_B T \ln a_R + \mu_R^\ominus + z_R e\phi \tag{22}$$

$$\mu_e = k_B T \ln a_e + \mu_e^\ominus - e\phi_e \tag{23}$$

($a_O = \prod_i a_i^{s_i}, \mu_O^\ominus = \sum_i s_i \mu_i^\ominus$) where μ_e is the Fermi level, which depends on ϕ_e and the electron activity $a_e = \gamma_e \tilde{c}_e$.

In equilibrium ($\mu_1 = \mu_2$), the interfacial voltage is given by the Nernst equation

$$\Delta\phi^{eq} = E^\ominus + \frac{k_B T}{n_c e} \ln \frac{a_O {a_e}^n}{a_R} \tag{24}$$

where $n_c = n$ and

$$E^\ominus = \frac{\mu_O^\ominus + n\mu_e^\ominus - \mu_R^\ominus}{ne} \tag{25}$$

is the standard half-cell potential. Out of equilibrium, the current $I = neR$ (per active site) is controlled by the activation overpotential,

$$\eta = \Delta\phi - \Delta\phi^{eq} = \frac{\Delta\mu}{ne} = \frac{\Delta G}{ne} \tag{26}$$

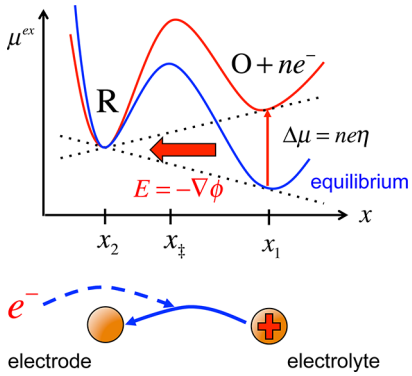

FIGURE 4. Landscape of excess chemical potential explored by the Faradaic reaction $O + ne^- \rightarrow R$ in Nernst equilibrium (blue) and after a negative overpotential $\eta = (\mu_2 - \mu_1)/(ne)$ is applied (red) to favor reduction, as illustrated below.

Specific models of charge transfer correspond to different choices of $\mu_\ddagger^{ex}$.

Generalized Butler–Volmer Kinetics. The standard phenomenological model of electrode kinetics is the Butler–Volmer equation,[28,45]

$$I = I_0(e^{-\alpha_c ne\eta/(k_B T)} - e^{\alpha_a ne\eta/(k_B T)}) \tag{27}$$

where I_0 is the exchange current. For a single-step charge-transfer reaction, the anodic and cathodic charge-transfer coefficients α_a and α_c satisfy $\alpha_a = 1 - \alpha$ and $\alpha_c = \alpha$ with a symmetry factor $0 < \alpha < 1$. The exchange current is typically modeled as $I_0 \propto c_O^{\alpha_a} c_R^{\alpha_c}$, but this is a dilute solution approximation.

In concentrated solutions, the exchange current is affected by configurational entropy and enthalpy, electrostatic correlations, coherency strain, and other nonidealities. For Li-ion batteries, only excluded volume has been considered, using[27,28] $I_0(c) \propto (c_s - c)^{\alpha_c} c^{\alpha_a}$. For fuel cells, many phenomenological models have been developed for electrocatalytic reactions with surface adsorption steps.[46–48] Electrocatalysis can also be treated by our formalism,[33] but here we focus on the elementary charge-transfer step and its coupling to phase transformations, which has no prior literature.

In order to generalize BV kinetics (Figure 4), we model the transition state

$$\mu_\ddagger^{ex} = k_B T \ln \gamma_\ddagger + (1 - \alpha)(z_O e\phi - ne\phi_e + \mu_O^\ominus + n\mu_e^\ominus) + \alpha(z_R e\phi + \mu_R^\ominus) \tag{28}$$

by averaging the standard chemical potential and electrostatic energy of the initial and final states, which assumes a constant electric field across the reaction coordinate x with $\alpha = (x_\ddagger - x_R)/(x_O - x_R)$. Substituting eq 28 into eq 7 using eq 24, we obtain eq 27 with

$$I_0 = \frac{k_0 ne(a_O a_e{}^n)^{1-\alpha} a_R{}^\alpha}{\gamma_\ddagger}$$

$$= k_0 ne(\tilde{c}_O \tilde{c}_e{}^n)^{1-\alpha} \tilde{c}_R{}^\alpha \left[\frac{(\gamma_O \gamma_e{}^n)^{1-\alpha} \gamma_R{}^\alpha}{\gamma_\ddagger}\right] \quad (29)$$

The factor in brackets is the thermodynamic correction for the exchange current.

Generalized BV kinetics (eqs 27 and 29) consistently applies chemical kinetics in concentrated solutions (eqs 10 and 12, respectively) to Faradaic reactions. In Li-ion battery models, $\Delta\phi^{eq}(c)$ is fitted to the open circuit voltage, and $I_0(c)$ and $D^{chem}(c)$ are fitted to discharge curves,[27,29,30] but these quantities are related by nonequilibrium thermodynamics.[9,26,35] Lai and Ciucci[49,50] also recognized this inconsistency and used eqs 5 and 24 in battery models, but they postulated a barrier of total (not excess) chemical potential, in contrast to eq 7, eq 29, and charge-transfer theory.

Generalized Marcus Kinetics. The microscopic theory of charge transfer, initiated by Marcus[52,53] and honored by the Nobel Prize in Chemistry,[54] provides justification for the BV equation and a means to estimate its parameters based on solvent reorganization.[45] Quantum mechanical formulations pioneered by Levich, Dogonadze, Marcus, Kuznetsov, and Ulstrup further account for Fermi statistics, band structure, and electron tunneling.[36] Most theories, however, make the dilute solution approximation by considering an isolated reaction complex.

In order to extend Marcus theory for concentrated solutions, our basic postulate (Figure 5) is that the Faradaic reaction eq 19 occurs when the excess chemical potential of the reduced state, deformed along the reaction coordinate by statistical fluctuations, equals that of the oxidized state (plus n electrons in the electrode) at the same point. (More precisely, charge transfer occurs at slightly lower energies due to quantum tunneling.[36,45]) Following Marcus, we assume harmonic restoring forces for structural relaxation (e.g., shedding of the solvation shell from a liquid or ion extraction from a solid) along the reaction coordinate x from the oxidized state at x_O to the reduced state at x_R:

$$\mu_1^{ex}(x) = \mu_O^\ominus + n\mu_e^\ominus + k_B T \ln(\gamma_O \gamma_e{}^n) + z_O e\phi - ne\phi_e + \frac{k_O}{2}(x - x_O)^2 \quad (30)$$

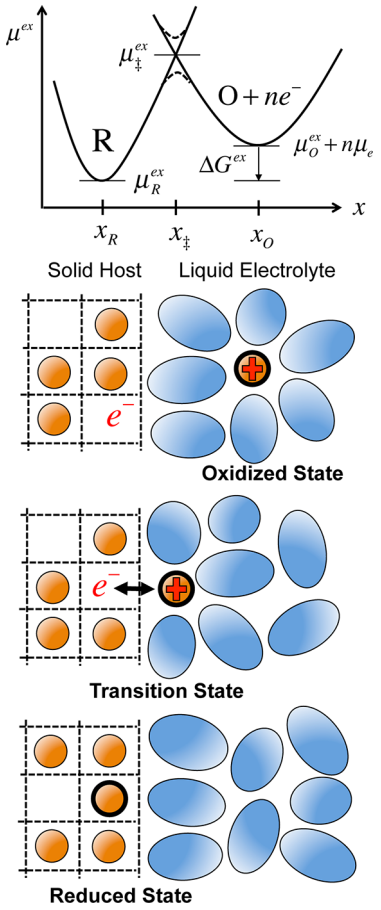

FIGURE 5. (top) The Faradaic reaction $O + ne^- \rightarrow R$ in concentrated solutions. Each state explores a landscape of excess chemical potential μ^{ex}. Charge transfer occurs where the curves overlap, or just below, by quantum tunneling (dashed curves). (bottom) Example of ion intercalation into a solid electrode from a liquid electrolyte.

$$\mu_2^{ex}(x) = \mu_R^\ominus + k_B T \ln \gamma_R + z_R e\phi + \frac{k_R}{2}(x - x_R)^2 \quad (31)$$

The Nernst equation, eq 24, follows by equating the total chemical potentials at the local minima, $\mu_1(x_O) = \mu_2(x_R)$ in equilibrium. The free energy barrier is set by the intersection of the excess chemical potential curves, $\mu_\ddagger^{ex} = \mu_1^{ex}(x_\ddagger) = \mu_2^{ex}(x_\ddagger)$, which determines the barrier position, $x = x_\ddagger$, and implies

$$\Delta G^{ex} = \mu_2^{ex}(x_R) - \mu_1^{ex}(x_O) = \frac{k_O}{2}(x_\ddagger - x_O)^2 - \frac{k_R}{2}(x_\ddagger - x_R)^2 \quad (32)$$

where ΔG^{ex} is the excess free energy change per reaction.

From eq 26, the overpotential is the total free energy change per charge transferred,

$$ne\eta = \Delta G = \Delta G^{ex} + k_B T \ln \frac{\tilde{c}_R}{\tilde{c}_O \tilde{c}_e{}^n} \quad (33)$$

In classical Marcus theory,[45,54] the overpotential is defined by $ne\eta = \Delta G^{ex}$ without the concentration factors required by nonequilibrium thermodynamics, which is

valid for charge-transfer reactions in bulk phases ($A^- + B \rightarrow A + B^-$) because the initial and final concentrations are the same, and thus $\Delta G = \Delta G^{ex} = \Delta G^\circ$ (standard free energy of reaction). For Faradaic reactions at interfaces, however, the concentrations of reactions and products are different, and eq 33 must be used. The missing "Nernst concentration term" in eq 33 has also been noted by Kuznetsov and Ulstrup (p 219 of ref 36).

In order to relate $\mu_\ddagger^{ex}$ to ΔG^{ex}, we solve eq 32 for $x_\ddagger$. In the simplest approximation, $k_O = k_R = k$, the barriers for the cathodic and anodic reactions,

$$\Delta G_c^{ex} = \mu_\ddagger^{ex} - \mu_1^{ex}(x_O) = \frac{\lambda}{4}\left(1+\frac{\Delta G^{ex}}{\lambda}\right)^2 \tag{34}$$

$$\Delta G_a^{ex} = \mu_\ddagger^{ex} - \mu_2^{ex}(x_R) = \frac{\lambda}{4}\left(1 - \frac{\Delta G^{ex}}{\lambda}\right)^2 \tag{35}$$

are related to the reorganization energy, $\lambda = (k/2)(x_O - x_R)^2$. These formulas contain the famous "inverted region" predicted by Marcus for isotopic exchange,[54] where (say) the cathodic rate, $k_c \propto e^{-\Delta G_c^{ex}}/(k_B T)$ reaches a minimum and increases again with decreasing driving force ΔG^{ex}, for $x_\ddagger < x_R$ in Figure 5a. This effect remains for charge transfer in concentrated bulk solutions, for example, $A^- + B \rightarrow A + B^-$. For Fardaic reactions, however, it is suppressed at metal electrodes, since electrons can tunnel through unoccupied conduction-band states, but can arise in narrow-band semiconductors.[36,53,54]

Substituting $\mu_\ddagger^{ex}$ into eq 7, we obtain

$$R = k_0\, e^{-\lambda/(4k_BT)}\, e^{-(\Delta G^{ex})^2/(4k_BT\lambda)}\, (\tilde{c}_O \tilde{c}_e^{\,n}\, e^{-\Delta G^{ex}/(2k_BT)} - \tilde{c}_R\, e^{\Delta G^{ex}/(2k_BT)}) \tag{36}$$

Using eq 33, we can relate the current to the overpotential,

$$I = I_0\, e^{-(ne\eta)^2/(4k_BT\lambda)}(e^{-\alpha ne\eta/(k_BT)} - e^{(1-\alpha)ne\eta/(k_BT)}) \tag{37}$$

via the exchange current,

$$I_0 = nek_0\, e^{-\lambda/(4k_BT)}(\tilde{c}_O \tilde{c}_e^{\,n})^{(3-2\alpha)/4}\tilde{c}_R^{\,(1+2\alpha)/4} \tag{38}$$

and symmetry factor,

$$\alpha = \frac{1}{2}\left(1 + \frac{k_BT}{\lambda}\ln\frac{\tilde{c}_O \tilde{c}_e^{\,n}}{\tilde{c}_R}\right) \tag{39}$$

In the typical case $\lambda \gg k_BT$, the current eq 37 is well approximated by the BV equation with $\alpha = 1/2$ at moderate overpotentials, $|\eta| > (k_BT/(ne))(\lambda/(k_BT))^{1/2}$, and nondepleted concentrations, $|\ln \tilde{c}| \ll (\lambda/(k_BT))$.

Comparing eq 38 with eq 29 for $\alpha \approx 1/2$, we can relate the reorganization energy to the activity coefficients defined above

$$\lambda \approx 4k_BT \ln \frac{\gamma_\ddagger}{(\gamma_O \gamma_e^{\,n} \gamma_R)^{1/2}} \tag{40}$$

For a dilute solution, the reorganization energy λ_0 can be estimated by the classical Marcus approximation, $\lambda_0 = \lambda_i + \lambda_o$, where λ_i is the "inner" or short-range contribution from structural relaxation (sum over normal modes) and λ_o is the "outer" or long-range contribution from the Born energy of solvent dielectric relaxation.[54,45] For polar solvents at room temperature, the large Born energy, $\lambda_o > 0.5n^2$ eV $\approx 20n^2 k_BT$ (at room temperature), implies that single-electron ($n = 1$), symmetric ($\alpha \approx 1/2$) charge transfer is favored. Quantum mechanical approximations of λ_0 are also available.[36] For a concentrated solution, we can estimate the thermodynamic correction, $\gamma_\ddagger^c$, for the entropy and enthalpy of the transition state and write

$$\gamma_\ddagger = \gamma_\ddagger^c\, e^{\lambda_0/(4k_BT)} \tag{41}$$

which can be used in either Marcus (eqs 37−40) or BV (eqs 27−29) kinetics. An example for ion intercalation is given below, eq 81, but first we need to develop a modeling framework for chemical potentials.

Nonequilibrium Chemical Thermodynamics

General Theory. In homogeneous bulk phases, activity coefficients depend on concentrations, but for reactions at an interface, concentration gradients must also play a role (Figure 1). The main contribution of this work has been to formulate chemical kinetics for inhomogeneous, nonequilibrium systems. The most general theory appears here for the first time, building on my lectures notes.[33]

The theory is based on the Gibbs free energy functional

$$G[\{c_i\}] = \int_V g\, dV + \oint_A \gamma_s\, dA = G_{bulk} + G_{surf} \tag{42}$$

with integrals over the bulk volume V and surface area A. The variational derivative,[55]

$$\frac{\delta G}{\delta c_i}(x) = \lim_{\varepsilon \to 0}\frac{G[c_i(y) + \varepsilon\delta_\varepsilon(y-x)] - G[c_i(y)]}{\varepsilon} \tag{43}$$

is the change in G to add a "continuum particle" $\delta(y-x)$ of species i at point x, where $\delta_\varepsilon(z) \rightarrow \delta(z)$ is a finite-size

approximation for a particle that converges weakly (in the sense of distributions) to the Dirac delta function, for example, $\delta_\varepsilon(z) = e^{-z^2/(2\varepsilon)}/\sqrt{2\pi\varepsilon}$. This is the consistent definition of diffusional chemical potential,[39,56]

$$\mu_i = \frac{\delta G}{\delta c_i} \tag{44}$$

If g depends on $\{c_i\}$ and $\{\nabla c_i\}$, then

$$\mu_i = \frac{\partial g}{\partial c_i} - \nabla\cdot\frac{\partial g}{\partial \nabla c_i} \tag{45}$$

The continuity of μ_i at the surface yields the "natural boundary condition",

$$\hat{n}\cdot\frac{\partial g}{\partial \nabla c_i} = \frac{\partial \gamma_s}{\partial c_i} \tag{46}$$

We can also express the activity variationally,

$$a_i = \exp\left(\frac{1}{k_B T}\frac{\delta G_{mix}}{\delta c_i}\right) \tag{47}$$

in terms of the free energy of mixing

$$G_{mix} = G_{bulk} - \sum_i \mu_i^\ominus \int_V c_i \, dV \tag{48}$$

which we define relative to the standard states of each species.

The simplest approximation for an inhomogeneous system is the Cahn–Hilliard[56] (or Landau–Ginzburg, or van der Waals[57]) gradient expansion,

$$g = \bar{g}(\{c_i\}) + \sum_i \left(\mu_i^\ominus c_i + \frac{1}{2}\sum_j \nabla\tilde{c}_i\cdot\kappa_{ij}\nabla\tilde{c}_j\right) \tag{49}$$

for which

$$\mu_i - \mu_i^\ominus = k_B T \ln a_i = \frac{\partial \bar{g}}{\partial c_i} - \sum_j \nabla\cdot\kappa_{ij}\nabla\frac{\tilde{c}_j}{c_j^\ominus} \tag{50}$$

where $\bar{g}$ is the homogeneous free energy of mixing and where κ_{ij} is a 2nd rank anisotropic tensor penalizing gradients in components i and j. (Higher-order derivative terms can also be added.[58,59])

With these definitions, eq 7 takes the variational form,

$$R = k_0\, e^{-\mu_\ddagger^{ex}/(k_B T)}\left[\exp\left(\sum_r \frac{s_r}{k_B T}\frac{\delta G}{\delta c_r}\right) - \exp\left(\sum_p \frac{s_p}{k_B T}\frac{\delta G}{\delta c_p}\right)\right] \tag{51}$$

for the general reaction, eq 3, in a concentrated solution. This is the fundamental expression of thermally activated reaction kinetics that is consistent with nonequilibrium thermodynamics. The reaction rate is a nonlinear function of the thermodynamic driving force,

$$\Delta\mu = \sum_p s_p\frac{\delta G}{\delta c_p} - \sum_r s_r\frac{\delta G}{\delta c_r} \tag{52}$$

This is the most general, variational definition of the free energy of reaction. For $|\Delta\mu| \ll k_B T$, the rate expression (51) can be linearized as

$$R \sim -k\Delta\mu, \quad k = \frac{k_0 e^{-\mu_\ddagger^{ex}/k_B T}}{k_B T} \tag{53}$$

but more generally, the forward and backward rates have exponential, Arrhenius dependence on the chemical potential barriers. The variational formulation of chemical kinetics, eq 51, can be applied to any type of reaction (Figure 6), as we now explain.

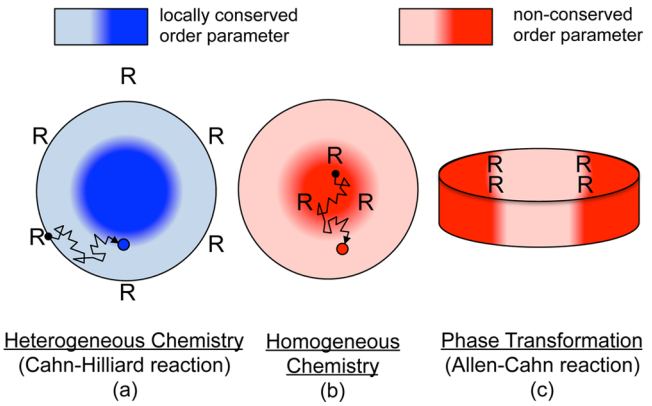

FIGURE 6. Types of reactions (R) in nonequilibrium chemical thermodynamics. (a) Heterogeneous chemistry at a surface, eq 54. (b) Homogeneous chemistry, eq 56, with diffusing species. (c) phase transformations or homogeneous reactions with immobile species, eq 58.

Heterogeneous Chemistry. At an interface, eq 51 provides a new reaction boundary condition[6,9,12,35]

$$s_i A_r \hat{n}\cdot\left(\vec{u}c_i - \frac{D_i c_i}{k_B T}\nabla\frac{\delta G}{\delta c_i}\right) = \pm R\left(\left\{\frac{\delta G}{\delta c_j}\right\}\right) \tag{54}$$

(+ for reactants, − for products; A_r = reaction site area) for the Cahn–Hilliard (CH) equation,[39]

$$\frac{\partial c_i}{\partial t} + \vec{u}\cdot\nabla c_i = \nabla\cdot\left(\frac{D_i c_i}{k_B T}\nabla\frac{\delta G}{\delta c_i}\right) \tag{55}$$

expressing mass conservation for the LIT flux, eq 5, with convection in a mean flow $\vec{u}$. For thermodynamic consistency, D_i is given by eq 18, which reduces eq 55 to the "modified" CH equation[58] in an ideal mixture.[26] This is the "Cahn–Hilliard reaction (CHR) model".

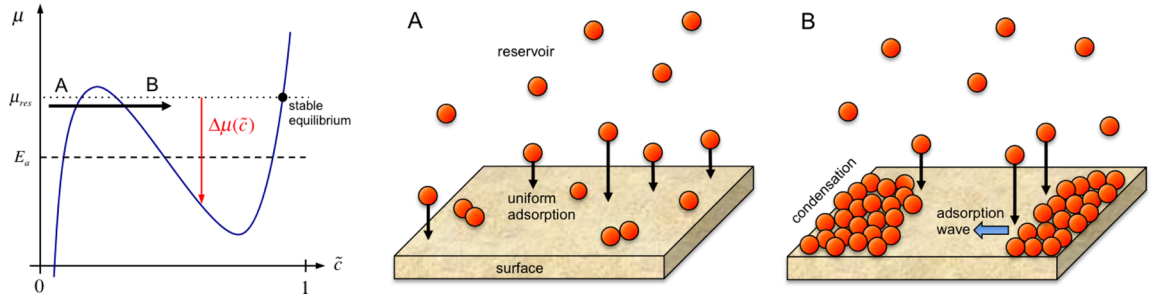

FIGURE 7. Surface adsorption with condensation when an empty surface is brought into contact with a reservoir ($\mu_{res} = \mu_1 = k_B T \ln a > E_{ads} = -k_B T \ln K^{\ominus}$). (left) Homogeneous chemical potential of the adsorbed species μ. (right) (A) Early stage uniform adsorption and (B) late-stage adsorption waves nucleated at edges, where the reaction is focused on advancing boundaries of the condensed phase.

Homogeneous Chemistry. For bulk reactions, eq 51 provides a new source term for the CH equation,

$$\frac{\partial c_i}{\partial t} + \vec{u}\cdot\nabla c_i = \nabla\cdot\left(\frac{D_i c_i}{k_B T}\nabla\frac{\delta G}{\delta c_i}\right) \mp \frac{c_s}{s_i} R\left(\left\{\frac{\delta G}{\delta c_j}\right\}\right) \qquad (56)$$

(c_s = reaction sites/volume). The Allen–Cahn equation[39] (AC) corresponds to the special case of an immobile reactant ($D_i = 0$, $\vec{u} = 0$) evolving according to linear kinetics, eq (53), although the exchange-rate prefactor k is usually taken to be constant, in contrast to our nonlinear theory. Equation 56 is the fundamental equation of nonequilibrium chemical thermodynamics. It unifies and extends the CH and AC equations via a consistent set of reaction-diffusion equations based on variational principles. Equation 54 is its integrated form for a reaction localized on a boundary.

Phase Transformations. In the case of an immobile reactant with two or more stable states, our general reaction-diffusion equation, eq 56, also describes thermally activated phase transformations. The immobile reactant concentration acts as a non-conserved order parameter, or phase field, representing different thermodynamic states of the same molecular substance. For example, if $\bar{g}(c)$ has two local equilibrium states, c_A and c_B, then

$$\xi = \frac{c - c_A}{c_A - c_B} \qquad (57)$$

is a phase field with minima at $\xi = 0$ and $\xi = 1$ satisfying

$$\frac{\partial \xi}{\partial t} = R\left(\frac{\delta G}{\delta \xi}\right) \qquad (58)$$

This is the "Allen–Cahn reaction (ACR) model", which is a nonlinear generalization of the AC equation for chemical kinetics.[7,9,12,33]

Example: Adsorption with Condensation. To illustrate the theory, we revisit surface adsorption with attractive forces, strong enough to drive adatom condensation (separation into high- and low-density phases) on the surface.[33] Applications may include water adsorption in concrete[60] or colloidal deposition in electrophoretic displays.[61] Following Cahn and Hilliard,[56] the simplest model is a regular solution of adatoms and vacancies with pair interaction energy Ω,

$$g = c_s\{k_B T[\tilde{c}\ln\tilde{c} + (1-\tilde{c})\ln(1-\tilde{c})] + \Omega\tilde{c}(1-\tilde{c}) + E_{ads}\tilde{c}\} + \frac{\kappa}{2}|\nabla\tilde{c}|^2 \qquad (59)$$

$$\mu = k_B T \ln\frac{\tilde{c}}{1-\tilde{c}} + \Omega(1-2\tilde{c}) + E_{ads} - \frac{\kappa}{c_s}\tilde{\nabla}^2\tilde{c} \qquad (60)$$

Below the critical point, $T < T_c = \Omega/(2k_B)$, the enthalpy of adatom attraction (third term, favoring phase separation $\tilde{c} = 0, 1$) dominates the configurational entropy of adatoms and vacancies (first two terms, favoring mixing $\tilde{c} = 1/2$). The gradient term controls spinodal decomposition and stabilizes phase boundaries of thickness $\lambda_b = (\kappa/(c_s\Omega))^{1/2}$ and interphasial tension $\gamma_b = (\kappa c_s\Omega)^{1/2}$. Using eq 15 to model the transition state with one excluded site, $s = 1$, the ACR model, eq 58, takes the dimensionless form,

$$\frac{\partial\tilde{c}}{\partial\tilde{t}} = K^{\ominus}a(1-\tilde{c}) - \tilde{c}\exp(\tilde{\Omega}(1-2\tilde{c}) - \tilde{\kappa}\tilde{\nabla}^2\tilde{c}) \qquad (61)$$

where $\tilde{t} = k_1 t$, $\tilde{\Omega} = \Omega/(k_B T) = 2T_c/T$, $\tilde{\kappa} = \kappa/(L^2 c_s k_B T)$ and $\tilde{\nabla} = L\nabla$ (with length scale L). This nonlinear PDE describes phase separation coupled to adsorption at an interface (Figure 7), controlled by the reservoir activity a. It resembles a reaction-diffusion equation, but there is no diffusion; instead, $-\tilde{\kappa}\tilde{\nabla}^2\tilde{c}$ is a gradient correction to the chemical potential, which nonlinearly affects the adsorption reaction rate. With modifications for charge transfer and coherency strain, a similar PDE describes ion intercalation in a solid host, driven by an applied voltage.

Nonequilibrium Thermodynamics of Electrochemical Systems

Background. We thus return to our original motivation, phase separation in Li-ion batteries (Figure 1). Three important papers in 2004 set the stage: Garcia et al.[62] formulated variational principles for electromagnetically active systems, which unify the CH equation with Maxwell's equations; Guyer et al.[64] represented the metal/electrolyte interface with a continuous phase field ξ evolving by AC kinetics; Han et al.[42] used the CH equation to model diffusion in LFP, leading directly to this work.

When the time is ripe for a new idea, a number of scientists naturally think along similar lines. As described in the Introduction, my group first reported phase-field kinetics (CHR and ACR)[12,43] and modified Poisson–Nernst–Planck (PNP) equations[41] in 2007, the generalized BV equation[35] in 2009, and the complete theory[9,33] in 2011. Independently, Lai and Ciucci also applied nonequilibrium thermodynamics to electrochemical transport[49] but did not develop a variational formulation. They proceeded to generalize BV kinetics[50,51] (citing Singh et al.[12]) but used μ in place of μ^{ex} and neglected $\gamma_{\ddagger}^{ex}$. Tang et al.[65] were the first to apply CHR to ion intercalation with coherency strain, but like Guyer et al.,[64] they assumed linear AC kinetics. Recently, Liang et al.[66] published the BV–ACR equation, claiming that "in contrast to all existing phase-field models, the rate of temporal phase-field evolution... is considered nonlinear with respect to the thermodynamic driving force". They cited my work[6,7,9,12] as a "boundary condition for a fixed electrode–electrolyte interface" (CHR) but overlooked the same BV–ACR equation for the depth-averaged ion concentration,[9,12] identified as a phase field for an open system.[7,9] They also set I_0 = constant, which contradicts chemical kinetics (see below).

Variational Electrochemical Kinetics. We now apply phase-field kinetics to charged species. The Gibbs free energy of ionic materials can be modeled as:[6,7,9,12,59,62,63,67]

$$G = G_{\text{mix}} + G_{\text{elec}} + G_{\text{surf}} + \sum_i \mu_i^{\ominus} \int_V c_i \, dV \tag{62}$$

$$G_{\text{mix}} = \int_V f(\vec{c}) \, dV + G_{\text{grad}} \tag{63}$$

$$G_{\text{grad}} = \frac{1}{2}\int_V (\nabla \vec{c} \cdot \kappa \nabla \vec{c} - \nabla\phi \cdot \varepsilon_p \nabla\phi + \sigma : \varepsilon) \, dV \tag{64}$$

$$G_{\text{elec}} = \int_V \rho_e \phi \, dV + \oint_A q_s \phi \, dA \tag{65}$$

where G_{grad} is the free energy associated with all gradients; G_{elec} is the energy of charges in the electrostatic potential of mean force, ϕ; $\vec{c}$ is the set of concentrations (including electrons for mixed ion/electron conductors); f is the homogeneous Helmholtz free energy density, ρ_e and q_s are the bulk and surface charge densities; ε_p is the permittivity tensor; and σ and ε are the stress and strain tensors. The potential ϕ acts as a Lagrange multiplier constraining the total ion densities[7,62] while enforcing Maxwell's equations for a linear dielectric material ($\delta G/\delta\phi = 0$),

$$-\nabla \cdot \varepsilon_p \nabla\phi = \rho_e = \sum_i z_i e c_i \tag{66}$$

$$-\hat{n} \cdot \varepsilon_p \nabla\phi = q_s \tag{67}$$

The permittivity can be a linear operator, for example, $\varepsilon_p = \varepsilon_0\left(1 - \ell_c^2 \nabla^2\right)$, to account for electrostatic correlations in ionic liquids[59] and concentrated electrolytes[35,68] (as first derived for counterion plasmas[69,70]). Modified PNP equations[35,41,49,50] correspond to eqs 55 and 66.

For elastic solids, the stress is given by Hooke's law, $\sigma_{ij} = C_{ijkl}\varepsilon_{kl}$, where C is the elastic constant tensor. The coherency strain,

$$\varepsilon_{ij} = \frac{1}{2}\left(\frac{\partial u_i}{\partial x_j} + \frac{\partial u_j}{\partial x_i}\right) - \sum_m \varepsilon_{ijm}^0 \tilde{c}_m \tag{68}$$

is the total strain due to compositional inhomogeneity (first term) relative to the stress-free inelastic strain (second term), which contributes to G_{mix}. In a mean-field approximation (Vegard's law), each molecule of species m exerts an independent strain ε_m^0 (lattice misfit between $\tilde{c}_m = 0$, 1 with $c_m^{\ominus} = c_s$). Since elastic relaxation (sound) is faster than diffusion and kinetics, we assume mechanical equilibrium, $\delta G/\delta\vec{u} = \nabla \cdot \sigma = 0$.

For Faradaic reactions, eq 19, the overpotential is the thermodynamic driving force for charge transfer,

$$ne\eta = \sum_j s_{j,R} \frac{\delta G}{\delta c_{j,R}} - \sum_i s_{i,O} \frac{\delta G}{\delta c_{i,O}} - n\frac{\delta G}{\delta c_e} \tag{69}$$

determined by the electrochemical potentials, $\mu_i = \delta G/\delta c_i$. For thermodynamic consistency, the diffusivities, eq 18, Nernst voltage, eq 24, and exchange current, eq 29, must depend on $\vec{c}$, $\nabla\vec{c}$, and σ via the variational activities, eq 47, given by

$$k_B T \ln a_i = \frac{\partial f}{\partial c_i} - \frac{\nabla \cdot \kappa \nabla \tilde{c}_i + \sigma : \varepsilon_i^0}{c_s} - \nabla\phi \cdot \frac{\partial \varepsilon_p}{\partial c_i} \nabla\phi \tag{70}$$

for the ionic model above. The Faradaic current density is

$$I = I_0 F\left(\frac{ne\eta}{k_B T}\right) \tag{71}$$

where

$$F(\tilde{\eta}) = \begin{cases} e^{-\alpha\tilde{\eta}} - e^{(1-\alpha)\tilde{\eta}} & \text{Butler–Volmer} \\ e^{-\tilde{\eta}^2/(4\tilde{\lambda})}(e^{-\alpha\tilde{\eta}} - e^{(1-\alpha)\tilde{\eta}}) & \text{Marcus} \end{cases} \tag{72}$$

and I_0 is given by either eq 29 or eqs 38–41, respectively ($\tilde{\lambda} = \lambda/(k_B T)$). The charge-transfer rate, $R = I/(ne)$, defines the CHR and ACR models, eqs 54–58, for electrochemical systems.

Example: Metal Electrodeposition. In models of electrodeposition[63,64] and electrokinetics,[71] the solid/electrolyte interface is represented by a continuous phase field, ξ, for numerical convenience (to avoid tracking a sharp interface). If the phase field evolves by reactions, however, it has physical significance as a chemical concentration. For example, consider electrodeposition, $M^{n+} + ne^- \rightarrow M$, of solid metal M from a binary electrolyte M^+A^- with dimensionless concentrations, $\xi = \tilde{c} = c/c_s$ and $\tilde{c}_\pm = c_\pm/c_0$, respectively. (The classical "phase field" is $\xi = \tilde{c}$.) In order to separate the metal from the electrolyte, we postulate

$$f = W[h(\tilde{c}) + \tilde{c}(\tilde{c}_+ + \tilde{c}_-)] + f_{ion}(\tilde{c}_+, \tilde{c}_-) \tag{73}$$

with $W \gg k_B T$, where $h = \tilde{c}^2(1-\tilde{c})^2$ is an arbitrary double-welled potential. For a dilute electrolyte, $f_{ion} = k_B T(\tilde{c}_+ \ln \tilde{c}_+ + \tilde{c}_- \ln \tilde{c}_-)$, without phase separation,[67] we include gradient energy only for the metal. The activities, eq 70, for reduced metal

$$c_s k_B T \ln a = W[h'(\tilde{c}) + \tilde{c}_+ + \tilde{c}_-] - \kappa\nabla^2\tilde{c} - \frac{\partial\varepsilon_p}{\partial\tilde{c}}|\nabla\phi|^2 \tag{74}$$

and metal cations

$$c_0 k_B T \ln a_+ = W\tilde{c} + k_B T \ln \tilde{c}_+ - \frac{\partial\varepsilon_p}{\partial\tilde{c}_+}|\nabla\phi|^2 \tag{75}$$

define the current density eq 71 via

$$I_0 = K_0 a^\alpha (a_+ a_e{}^n)^{1-\alpha}, \quad K_0 = \frac{nek_0 c_s}{\gamma_\ddagger} \tag{76}$$

$$\eta = \frac{k_B T}{ne} \ln \frac{a}{a_+ a_e{}^n} - E^\ominus \tag{77}$$

Note that the local potential for electrons and ions is unique ($\phi = \phi_e$, $\Delta\phi = 0$), but integration across the diffuse interface yields the interfacial voltage.

The ACR equation, eq 58, for $\xi = \tilde{c}$ using eqs 71–77 differs from prior phase-field models of electrodeposition.[64,66] Equation 76 has the thermodynamically consistent dependence on reactant activities (rather than I_0 = constant). Coupled with generalized PNP equations, eq 56, for $\tilde{c}_\pm$, our theory also describes Frumkin corrections to Butler–Volmer kinetics[72,73] and electro-osmotic flows[35,71] associated with double-layer diffuse charge. The permittivity $\varepsilon_p(\tilde{c}, \tilde{c}_\pm)$ depends on the metal concentration, interpolating between metal ($\varepsilon_p^M, \tilde{c} = 1$) and bulk electrolyte ($\varepsilon_p^b, \tilde{c} = 0$) values[63] with a minimum (ε_p^S, $\tilde{c} \approx 1/2$) for the Stern layer,[72] as well as the ionic concentrations, $\varepsilon_p \propto \varepsilon_0(1 + \alpha_+\tilde{c}_+ + \alpha_-\tilde{c}_-)$ where $\alpha_\pm < 0$ are the excess polarizabilities.[74,75] Dielectric saturation in large fields, $\varepsilon_p(|\nabla\phi|)$, can also be included.[35] The charge density includes the conduction electrons and solid metal ions, $\rho_e = ze(c_+ - c_-) + z_M e(c_M - c_e)$. Neglecting band structure variations, we can set $a_e = \tilde{c}_e$ and $a_M = \tilde{c}_M$. The theory thus predicts diffuse-charge profiles on both sides of the interface, involving ions and electrons,[76] during Faradaic reactions.

Example: Ion Intercalation. Hereafter, we neglect double layers and focus on solid thermodynamics. Consider cation intercalation, $A^{n+} + B + ne^- \rightarrow AB$, from an electrolyte reservoir (a_O = constant) into a conducting solid B (a_e = constant) as a neutral polaron ($c_R = c(x,t)$, $z_R = 0$). The overpotential eq 69 takes the simple form

$$ne\eta = \frac{\delta G}{\delta c} - (\mu_O + n\mu_e) = \frac{\delta G_{mix}}{\delta c} + ne\Delta\Phi \tag{78}$$

where

$$\Delta\Phi = \Delta\phi - E^\ominus - \frac{k_B T}{ne} \ln a_O a_e^n \tag{79}$$

is the interfacial voltage relative to the ionic standard state. The equilibrium voltage is

$$ne\Delta\Phi_{eq} = -k_B T \ln a = -\frac{\delta G_{mix}}{\delta c} \tag{80}$$

Note that potentials can be shifted for convenience: Bai et al.[9] and Ferguson and Bazant[26] set $\mu^\ominus = 0$ for ions, so $\mu = k_B T \ln a = \delta G_{mix}/\delta c$; Cogswell and Bazant[7] defined "$\Delta\phi$" = $\Delta\Phi$ and shifted g by $-c\Delta\Phi$, so $e\eta = \delta G/\delta c$.

Our surface adsorption model, eq 59, can be adapted for ion intercalation by setting $E_a = e\Delta\Phi$. If the transition state excludes s sites (where $s > 1$ could account for the A^{n+} solvation shell) and has strain $-\varepsilon_\ddagger$, then its activity coefficient, eq 41, is

$$\gamma_\ddagger = (1-\tilde{c})^{-s} \exp(-\tilde{\sigma} : \varepsilon_\ddagger + \tilde{\lambda}_0/4) \tag{81}$$

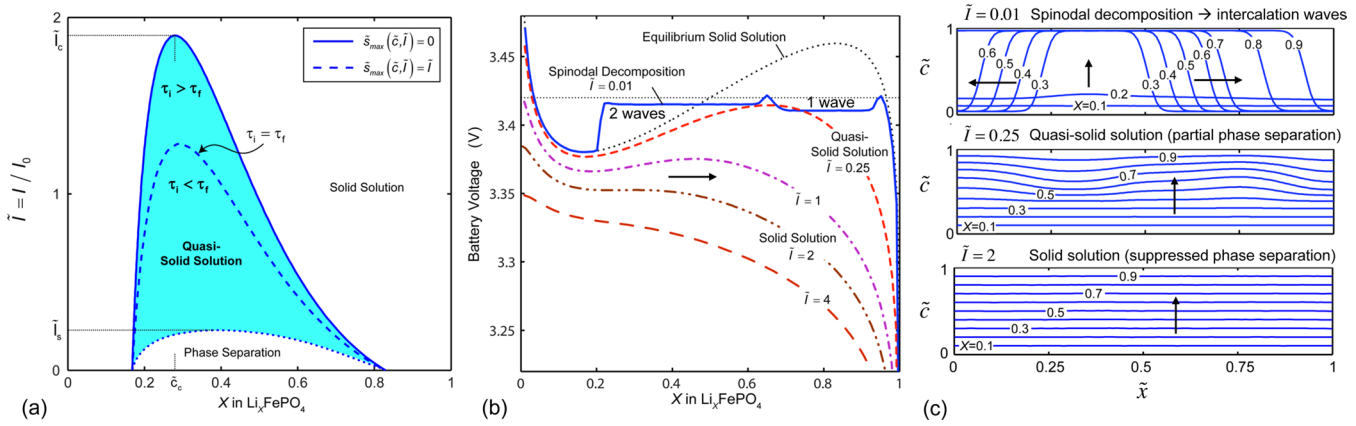

FIGURE 8. Suppression of phase separation at constant current in a Li-ion battery nanoparticle (ACR model without coherency strain or surface wetting).[9] (a) Linear stability diagram for the homogeneous state versus dimensionless current, $\tilde{I} = I/I_0$ ($\tilde{c} = 0.5$), and state of charge X. (b) Battery voltage versus X with increasing $\tilde{I}$. (c) Concentration profiles, spinodal decomposition at $\tilde{I} = 0.01$ leading to intercalation waves (Figure 1(c)), quasi-solid solution at $\tilde{I} = 0.25$, and homogeneous filling at $\tilde{I} = 2$.

where $\tilde{\lambda}_0 = \lambda_0/(k_B T)$ and $\tilde{\sigma} = \sigma/(c_s k_B T)$. The exchange current, eq 29, is

$$I_0 = nek(\tilde{c})\tilde{c}^{\alpha}(1-\tilde{c})^{s-\alpha}\exp(\tilde{\sigma}:\Delta\varepsilon + \alpha\tilde{\Omega}(1-2\tilde{c}) - \alpha\tilde{\nabla}\cdot\tilde{\kappa}\tilde{\nabla}\tilde{c}) \tag{82}$$

$$k(\tilde{c}) = k_0 c_s (a_+ a_e^{\eta}(\tilde{c}))^{1-\alpha}\, e^{-\tilde{\lambda}_0/4} \tag{83}$$

where a_+ is the ionic activity in the electrolyte and $\Delta\varepsilon = \varepsilon_{\ddagger} - \alpha\varepsilon^0$ is the activation strain.[77] For semiconductors, the electron activity $a_e = e^{\Delta E_f/(k_B T)}$ depends on $\tilde{c}$, if the intercalated ion shifts the Fermi level by donating an electron to the conduction band, for example, $\Delta E_f \propto (1+\beta\tilde{c})^{2/d}$ for free electrons in d dimensions (as in $LiWO_3$ with $d = 3$[78]).

Application to Li-Ion Battery Electrodes

Allen–Cahn Reaction Model. The three-dimensional CHR model eqs 54–55 with current density $I = neR$ given by eqs 71 and 82 describes ion intercalation in a solid particle from an electrolyte reservoir. In nanoparticles, solid diffusion times (milliseconds to seconds) are much shorter than discharge times, so a reaction-limited ACR model is often appropriate. In the case of LFP nanoparticles, strong crystal anisotropy leads to a two-dimensional ACR model over the active (010) facet by depth averaging over N_s sites in the [010] direction.[9,12] For particle sizes below 100 nm, the concentration tends to be uniform in [010] due to the fast diffusion[13] (uninhibited by Fe anti-site defects[16]) and elastically unfavorable phase separation.[7]

Using eqs 71 and 82 with isotropic $\tilde{\kappa}$, a_e = constant, $\varepsilon_{\ddagger} = \alpha\varepsilon_0$, $\alpha = 1/2$, and $s = 1$, the ACR equation, eq 58, takes the simple dimensionless form,[7,9]

$$\frac{\partial\tilde{c}}{\partial\tilde{t}} = \tilde{I}_0 F(\tilde{\mu} + \Delta\tilde{\Phi}) \tag{84}$$

$$\tilde{\mu} = \ln\frac{\tilde{c}}{1-\tilde{c}} + \tilde{\Omega}(1-2\tilde{c}) - \tilde{\kappa}\tilde{\nabla}^2\tilde{c} + \tilde{\sigma}:\varepsilon \tag{85}$$

$$\tilde{I}_0 = \sqrt{\tilde{c}(1-\tilde{c})}\exp\left[\frac{1}{2}\left(\tilde{\Omega}(1-2\tilde{c}) - \tilde{\kappa}\tilde{\nabla}^2\tilde{c}\right)\right] \tag{86}$$

where $\Delta\tilde{\Phi} = ne\Delta\Phi/(k_B T)$, $\tilde{t} = N_s k t$. The total current integrated over the active facet

$$\tilde{I}(\tilde{t}) = \int_{\tilde{A}} \frac{\partial\tilde{c}}{\partial\tilde{t}}\, d\tilde{x}\, d\tilde{y} \tag{87}$$

is controlled while solving for $\Delta\tilde{\Phi}(\tilde{t})$ (as in Figure 8) or vice versa (where $\tilde{A}$ is the dimensionless surface area of the active facet).

Intercalation Waves and Quasi-Solid Solutions. The theory predicts a rich variety of new intercalation mechanisms. A special case of the CHR model[12] is isotropic diffusion-limited intercalation[27,28] with a shrinking-core phase boundary,[29,30] but the reaction-limited ACR model also predicts intercalation waves (or "domino cascades"[15]), sweeping across the active facet, filling the crystal layer by layer (Figure 1c).[7,9,12,34,65] Intercalation waves result from spinodal decomposition or nucleation at surfaces[9] and trace out the voltage plateau at low current (Figure 8).

The theory makes other surprising predictions about electrochemically driven phase transformations. Singh et al.[12] showed that intercalation wave solutions of the ACR equation only exist over a finite range of thermodynamic driving force. Based on bulk free energy calculations, Malik et al.[10] argued for a "solid solution pathway" without phase separation under applied current, but Bai et al.[9] used the BV–ACR model to show that phase separation is suppressed by activation overpotential at high current (Figure 8), due to the reduced area for

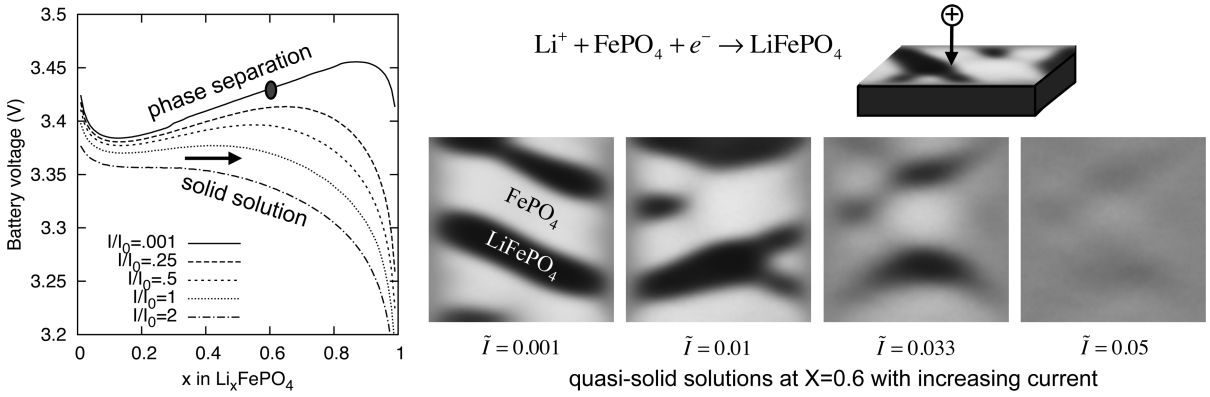

FIGURE 9. ACR simulations of galvanostatic discharge in a 100 nm Li_xFePO_4 nanoparticle.[7] As the current is increased, transient quasi-solid solutions (images from the shaded region) transition to homogeneous filling for $\tilde{I} > 0.1$, as phase separation is suppressed.

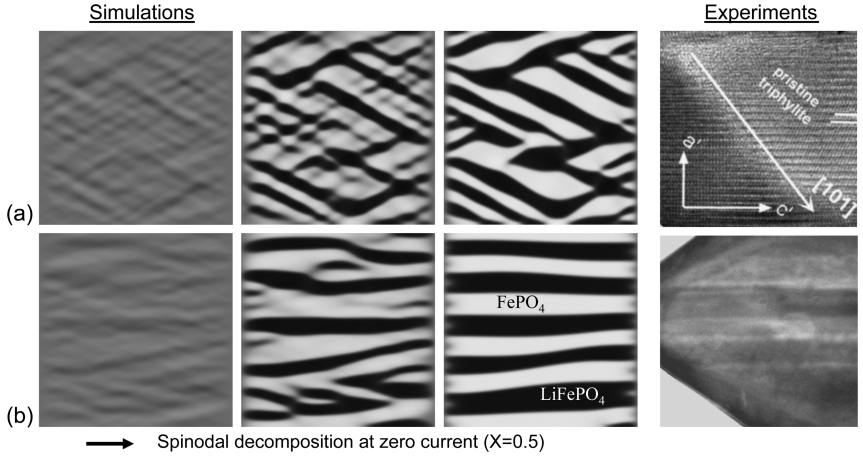

FIGURE 10. Phase separation of a 500 nm particle of $Li_{0.5}FePO_4$ into Li-rich (black) and Li-poor phases (white) at zero current in ACR simulations,[7] compared with *ex situ* experimental images.[31,32] (a) Coherent phase separation with [101] interfaces. (b) Semicoherent phase separation, consistent with observed {100} microcracks.[31]

intercalation on the phase boundary (Figure 1c). Linear stability analysis of homogeneous filling predicts a critical current, on the order of the exchange current, above which phase separation by spinodal decomposition is impossible. Below this current, the homogeneous state is unstable over a range of concentrations (smaller than the zero-current spinodal gap), but for large currents, the time spent in this region is too small for complete phase separation. Instead, the particle passes through a transient "quasi-solid solution" state, where its voltage and concentration profile resemble those of a homogeneous solid solution. When nucleation is possible (see below), a similar current dependence is also observed.

For quantitative interpretation of experiments, it is essential to account for the elastic energy.[7] Coherency strain is a barrier to phase separation (Figure 9), which tilts the voltage plateau (compared with Figure 8) and reduces the critical current, far below the exchange current. An unexpected prediction is that phase separation rarely occurs *in situ* during battery operation in LFP nanoparticles, which helps to explain their high rate capability and extended lifetime.[7,9]

Phase separation occurs at low currents and can be observed *ex situ* in partially filled particles (Figure 10). Crystal anisotropy leads to striped phase patterns in equilibrium,[17−19] whose spacing is set by the balance of elastic energy (favoring short wavelengths at a stress-free boundary) and interfacial energy (favoring long wavelengths to minimize interfacial area).[7] Stanton and Bazant[19] predicted that simultaneous positive and negative eigenvalues of ε_0 make phase boundaries tilt with respect to the crystal axes. In LFP, lithiation causes contraction in the [001] direction and expansion in the [100] and [010] directions.[31] Depending on the degree of coherency, Cogswell and Bazant[7] predicted phase morphologies in excellent agreement with experiments (Figure 10) and inferred the gradient penalty κ and the $LiFePO_4/FePO_4$ interfacial tension (beyond the reach of molecular simulations) from the observed stripe spacing.

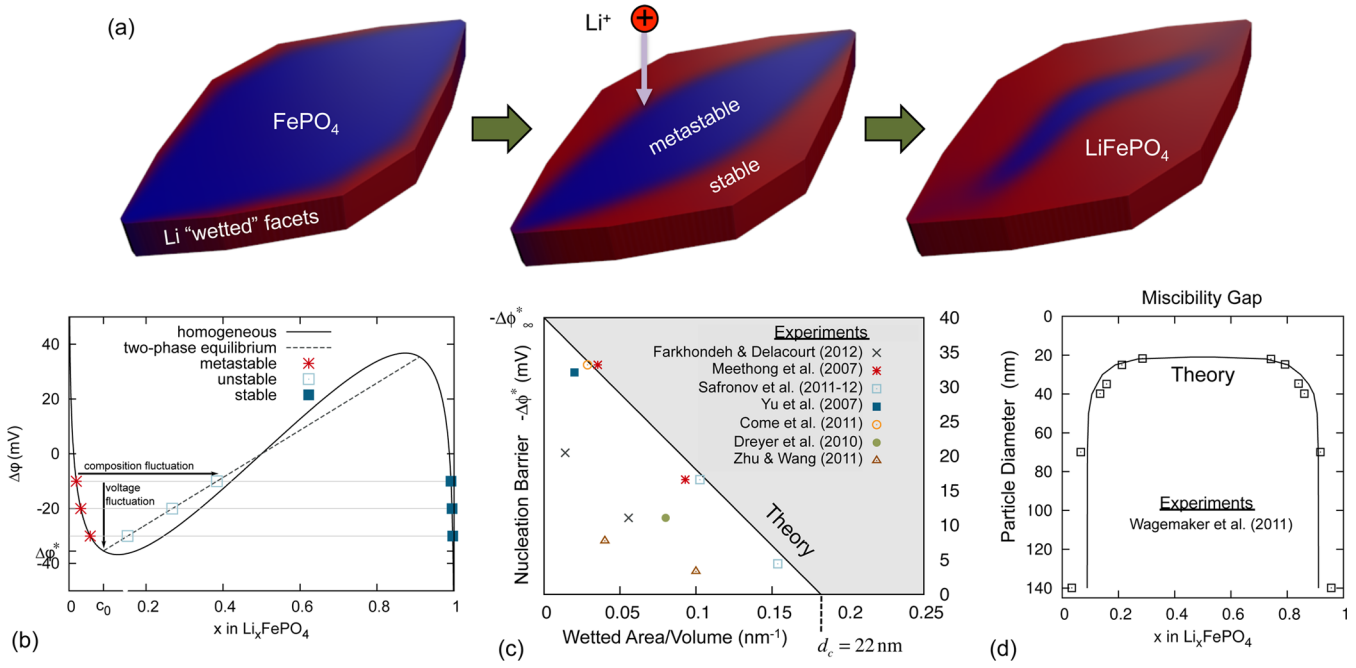

FIGURE 11. (a) ACR simulation of galvanostatic nucleation in a realistic LFP nanoparticle shape (C3)[76] with a 150 nm × 76 nm top (010) active facet.[8] Surface "wetting" of the side facets by lithium nucleates intercalation waves that propagate across the particle (while bending from coherency strain) after the voltage exceeds the coherent miscibility limit. (b) Discharge plot indicating nucleation by fluctuations in voltage or composition.[8] (c) Collapse of experimental data for the nucleation voltage by the theory, without any fitting parameters.[8] (d) Size dependence of the miscibility gap, fitted by the theory.[7]

Driven Nucleation and Growth. The theory can also quantitatively predict nucleation dynamics driven by chemical reactions. Nucleation is perhaps the least understood phenomenon of thermodynamics. In thermal phase transitions, such as boiling or freezing, the critical nucleus is controlled by random heterogeneities, and its energy is overestimated by classical spherical droplet nucleation theory. Phase-field models address this problem but often lack sufficient details to be predictive.

For battery nanoparticles, nucleation turns out to be more tractable, in part because the current and voltage can be more precisely controlled than heat flux and temperature. More importantly, the critical nucleus has a well-defined form, set by the geometry, due to strong surface "wetting" of crystal facets by different phases. Cogswell and Bazant[8] showed that nucleation in binary solids occurs at the coherent miscibility limit, as a surface layer becomes unstable and propagates into the bulk. The nucleation barrier, $E_b = -e\Delta\Phi$ is set by coherency strain energy (scaling with volume) in large particles and reduced by surface energy (scaling with area) in nanoparticles. The barrier thus decays with the wetted area-to-volume ratio, A/V, and vanishes at a critical size, below which nanoparticles remain homogeneous in the phase of lowest surface energy.

The agreement between theory and experiment, without fitting any parameters, is impressive (Figure 11). Using our prior ACR model[7] augmented only by *ab initio* calculated surface energies (in eq 46), the theory is able to collapse E_b data for LFP versus A/V, which lie either on the predicted line or below (e.g., from heterogeneities, lowering E_b, or missing the tiniest nanoparticles, lowering A/V).[8] This resolves a major controversy, since the data had seemed inconsistent ($E_b = 2.0-37$ mV), and some had argued for[12,22,77] and others against the possibility of nucleation (using classical droplet theory).[10] The new theory also predicts that the nucleation barrier (Figure 11c) and miscibility gap (Figure 11d) vanish at the same critical size, $d_c \approx 22$ nm, consistent with separate Li-solubility experiments.[11]

Mosaic Instability and Porous Electrodes. These findings have important implications for porous battery electrodes, consisting of many phase-separating nanoparticles. The prediction that small particles transform before larger ones is counterintuitive (since larger particles have more nucleation sites) and opposite to classical nucleation theory. The new theory could be used to predict mean nucleation and growth rates in a simple statistical model[77] that fits current transients in LFP[22] and guide extensions to account for the particle size distribution.

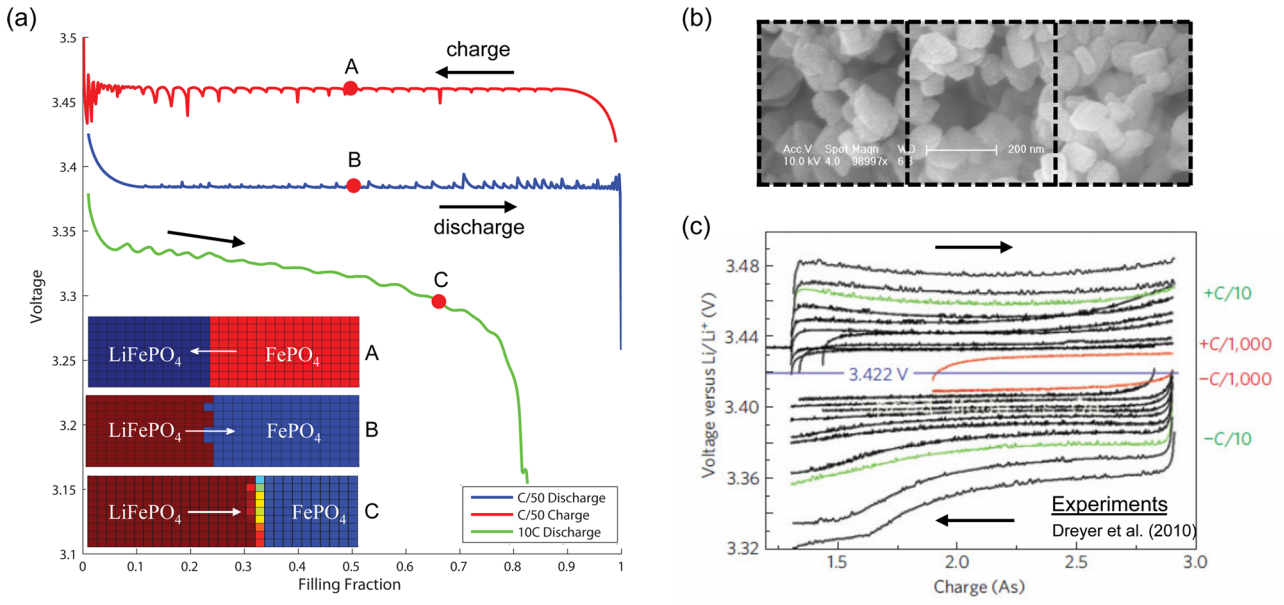

FIGURE 12. Finite-volume simulations of a porous LFP cathode (Ferguson and Bazant[26]). (a) Voltage versus state of charge at different rates with profiles of the mean solid Li concentration (A−C), separator on the left, current collector on the right. (b) SEM image of LFP nanoparticles represented by three finite volumes (P. Bai). (c) Experiments revealing a zero-current gap between noisy charge and discharge voltage plateaus (From Dreyer et al.[23]).

Discrete, random transformations also affect voltage transients. Using the CHR model[6] for a collection of particles in a reservoir, Burch[25] discovered the "mosaic instability", whereby particles switch from uniform to sequential filling after entering the miscibility gap. Around the same time, Dreyer et al.[23] published a simple theory of the same effect (neglecting phase separation within particles) supported by experimental observations of voltage gap between charge/discharge cycles in LFP batteries (Figure 12c), as well as pressure hysteresis in ballon array.[24]

The key ingredient missing in these models is the transport of ions (in the electrolyte) and electrons (in the conducting matrix), which mediates interactions between nanoparticles and becomes rate limiting at high current. Conversely, the classical description of porous electrodes, pioneered by Newman,[27,28] focuses on transport but mostly neglects the thermodynamics of the active materials,[26,50] for example, fitting[29] rather than deriving[9,23,49,51] the voltage plateau in LFP. These approaches are unified by nonequilibrium chemical thermodynamics.[26] Generalized porous electrode theory is constructed by formally volume averaging over the microstructure to obtain macroscopic reaction-diffusion equations of the form eq 56 for three overlapping continua, the electrolyte, conducting matrix, and active material, each containing a source/sink for Faradaic reactions, integrated over the internal surface of the active particles, described by the CHR or ACR model.

The simplest case is the "pseudo-capacitor approximation" of fast solid relaxation (compared with reactions and macroscopic transport), where the active particles remain homogeneous. Using our model for LFP nanoparticles,[7] the porous electrode theory predicts the zero-current voltage gap, without any fitting (Figure 12). (Using the mean particle size, the gap is somewhat too large, but this can be corrected by size-dependent nucleation (Figure 11), implying that smaller particles were preferentially cycled in the experiments.) Voltage fluctuations at low current correspond to discrete sets of transforming particles. For a narrow particle size distribution, mosaic instability sweeps across the electrode from the separator as a narrow reaction front (Figure 12a, inset). As the current is increased, the front width grows, and the active material transforms more uniformly across the porous electrode, limited by electrolyte diffusion. A wide particle size distribution also broadens the reaction front, as particles transform in order of increasing size. These examples illustrate the complexity of phase transformations in porous media driven by chemical reactions.

Conclusion

This Account describes a journey along the "middle way",[78] searching for organizing principles of the mesoscopic domain between individual atoms and bulk materials. The motivation to understand phase behavior in Li-ion battery nanoparticles gradually led to a theory of collective kinetics at length and time scales in the "middle", beyond the reach of both molecular simulations and macroscopic continuum models. The work leveraged advances in *ab initio*

quantum-mechanical calculations and nanoscale imaging but also required some new theoretical ideas.

Besides telling the story, this Account synthesizes my work as a general theory of chemical physics, which transcends its origins in electrochemistry. The main result, eq 56, generalizes the Cahn–Hilliard and Allen–Cahn equations for reaction-diffusion phenomena. The reaction rate is a nonlinear function of the species activities and the free energy of reaction (eq 7) via variational derivatives of the Gibbs free energy functional (eq 51), which are consistently defined for nonequilibrium states, for example, during a phase separation. For charged species, the theory generalizes the Poisson–Nernst–Planck equations of ion transport, the Butler–Volmer equation of electrochemical kinetics (eq 29), and the Marcus theory of charge transfer (eq 37) for concentrated electrolytes and ionic solids.

As its first application, the theory has predicted new intercalation mechanisms in phase-separating battery materials, exemplified by LFP: intercalation waves in anisotropic nanoparticles at low currents (Figure 8); quasi-solid solutions and suppressed phase separation at high currents (Figure 9); relaxation to striped phases in partially filled particles (Figure 10); size-dependent nucleation by surface wetting (Figure 11); and mosaic instabilities and reaction fronts in porous electrodes (Figure 12). These results have some unexpected implications, for example, that battery performance may be improved with elevated currents and temperatures, wider particle size distributions, and coatings to alter surface energies. The model successfully describes phase behavior of LFP cathodes, and my group is extending it to graphite anodes ("staging" of Li intercalation with ≥ 3 stable phases) and air cathodes (electrochemical growth of Li_2O_2).

The general theory may find many other applications in chemistry and biology. For example, the adsorption model (Figure 7) could be adapted for the deposition of charged colloids on transparent electrodes in electrophoretic displays. The porous electrode model (Figure 12) could be adapted for sorption/desorption kinetics in nanoporous solids, for example, for drying cycles of cementitious materials, release of shale gas by hydraulic fracturing, carbon sequestration in zeolites, or ion adsorption and impulse propagation in biological cells. The common theme is the coupling of chemical kinetics with nonequilibrium thermodynamics.

This work was supported by the National Science Foundation under Contracts DMS-0842504 and DMS-0948071 and by the MIT Energy Initiative and would not have been possible without my postdoctoral associates (D. A. Cogswell, G. Singh) and students (P. Bai, D. Burch, T. R. Ferguson, E. Khoo, R. Smith, Y. Zeng). P. Bai noted the Nernst factor in eq 39.

Note Added after ASAP Publication. This paper was posted to the WEB on March 22, 2013 with errors in several equations. The revised version was reposted on April 11, 2013.

BIOGRAPHICAL INFORMATION

Martin Z. Bazant received his B.S. (Physics, Mathematics, 1992) and M.S. (Applied Mathematics, 1993) from the University of Arizona and Ph.D. (Physics, 1997) from Harvard University. He joined the faculty at MIT in Mathematics in 1998 and Chemical Engineering in 2008. His honors include an Early Career Award from the Department of Energy (2003), Brilliant Ten from *Popular Science* (2007), and Paris Sciences Chair (2002, 2007) and Joliot Chair (2008, 2012) from ESPCI (Paris, France).

FOOTNOTES

*E-mail: bazant@mit.edu.
The author declares no competing financial interest.

REFERENCES

1 Padhi, A.; Nanjundaswamy, K.; Goodenough, J. Phospho-olivines as positive-electrode materials for rechargeable lithium batteries. *J. Electrochem. Soc.* **1997**, *144*, 1188–1194.

2 Tarascon, J.; Armand, M. Issues and challenges facing rechargeable lithium batteries. *Nature* **2001**, *414*, 359–367.

3 Kang, B.; Ceder, G. Battery materials for ultrafast charging and discharging. *Nature* **2009**, *458*, 190–193.

4 Tang, M.; Carter, W. C.; Chiang, Y.-M. Electrochemically driven phase transitions in insertion electrodes for lithium-ion batteries: Examples in lithium metal phosphate olivines. *Annu. Rev. Mater. Res.* **2010**, *40*, 501–529.

5 Meethong, N.; Huang, H.-Y. S.; Carter, W. C.; Chiang, Y.-M. Size-dependent lithium miscibility gap in nanoscale $Li_{1-x}FePO_4$. *Electrochem. Solid-State Lett.* **2007**, *10*, A134–A138.

6 Burch, D.; Bazant, M. Z. Size-dependent spinodal and miscibility gaps for intercalation in nanoparticles. *Nano Lett.* **2009**, *9*, 3795–3800.

7 Cogswell, D. A.; Bazant, M. Z. Coherency strain and the kinetics of phase separation in $LiFePO_4$ nanoparticles. *ACS Nano* **2012**, *6*, 2215–2225.

8 Cogswell, D. A.; Bazant, M. Z. Theory of nucleation in nanoparticles. *Nano Letters*, submitted.

9 Bai, P.; Cogswell, D.; Bazant, M. Z. Suppression of phase separation in $LiFePO_4$ nanoparticles during battery discharge. *Nano Lett.* **2011**, *11*, 4890–4896.

10 Malik, R.; Zhou, F.; Ceder, G. Kinetics of non-equilibrium lithium incorporation in $LiFePO_4$. *Nat. Mater.* **2011**, *10*, 587–590.

11 Wagemaker, M.; Singh, D. P.; Borghols, W. J.; Lafont, U.; Haverkate, L.; Peterson, V. K.; Mulder, F. M. Dynamic solubility limits in nanosized olivine $LiFePO_4$. *J. Am. Chem. Soc.* **2011**, *133*, 10222–10228.

12 Singh, G.; Burch, D.; Bazant, M. Z. Intercalation dynamics in rechargeable battery materials: General theory and phase-transformation waves in $LiFePO_4$. *Electrochim. Acta* **2008**, *53*, 7599–7613arXiv:0707.1858v1 [cond-mat.mtrl-sci] (2007).

13 Morgan, D.; der Ven, A. V.; Ceder, G. Li conductivity in Li_xMPO_4 (M = Mn, Fe, Co, Ni) olivine materials. *Electrochem. Solid State Lett.* **2004**, *7*, A30–A32.

14 Laffont, L.; Delacourt, C.; Gibot, P.; Wu, M. Y.; Kooyman, P.; Masquelier, C.; Tarascon, J. M. Study of the $LiFePO_4/FePO_4$ two-phase system by high-resolution electron energy loss spectroscopy. *Chem. Mater.* **2006**, *18*, 5520–5529.

15 Delmas, C.; Maccario, M.; Croguennec, L.; Cras, F. L.; Weill, F. Lithium deintercalation of $LiFePO_4$ nanoparticles via a domino-cascade model. *Nat. Mater.* **2008**, *7*, 665–671.

16 Malik, R.; Burch, D.; Bazant, M.; Ceder, G. Particle size dependence of the ionic diffusivity. *Nano Lett.* **2010**, *10*, 4123–4127.

17 Meethong, N.; Huang, H. Y. S.; Speakman, S. A.; Carter, W. C.; Chiang, Y. M. Strain accommodation during phase transformations in olivine-based cathodes as a materials

selection criterion for high-power rechargeable batteries. *Adv. Funct. Mater.* **2007**, *17*, 1115–1123.

18 der Ven, A. V.; Garikipati, K.; Kim, S.; Wagemaker, M. The role of coherency strains on phase stability in Li_xFePO_4: Needle crystallites minimize coherency strain and overpotential. *J. Electrochem. Soc.* **2009**, *156*, A949–A957.

19 Stanton, L. G.; Bazant, M. Z. Phase separation with anisotropic coherency strain. *arXiv* **2012**, No. arXiv:1202.1626v1.

20 der Ven, A. V.; Wagemaker, M. Effect of surface energies and nano-particle size distribution on open circuit voltage of Li-electrodes. *Electrochem. Commun.* **2009**, *11*, 881–884.

21 Wagemaker, M.; Mulder, F. M.; der Ven, A. V. The role of surface and interface energy on phase stability of nanosized insertion compounds. *Adv. Mater.* **2009**, *21*, 2703–2709.

22 Oyama, G.; Yamada, Y.; Natsui, R.; Nishimura, S.; Yamada, A. Kinetics of nucleation and growth in two-phase electrochemical reaction of Li_xFePO_4. *J. Phys. Chem. C* **2012**, *116*, 7306–7311.

23 Dreyer, W.; Jamnik, J.; Guhlke, C.; Huth, R.; Moskon, J.; Gaberscek, M. The thermo-dynamic origin of hysteresis in insertion batteries. *Nat. Mater.* **2010**, *9*, 448–453.

24 Dreyer, D.; Guhlke, C.; Huth, R. The behavior of a many-particle electrode in a lithium-ion battery. *Phys. D* **2011**, *240*, 1008–1019.

25 Burch, D. Intercalation Dynamics in Lithium-Ion Batteries, Ph.D. Thesis in Mathematics, Massachusetts Institute of Technology, 2009.

26 Ferguson, T. R.; Bazant, M. Z. Non-equilibrium thermodynamics of porous electrodes. *J. Electrochem. Soc.* **2012**, *159*, A1967–A1985.

27 Doyle, M.; Fuller, T. F.; Newman, J. Modeling of galvanostatic charge and discharge of the lithium/polymer/insertion cell. *J. Electrochem. Soc.* **1993**, *140*, 1526–1533.

28 Newman, J. *Electrochemical Systems*, 2nd ed.; Prentice-Hall, Inc.: Englewood Cliffs, NJ, 1991.

29 Srinivasan, V.; Newman, J. Discharge model for the lithium iron-phosphate electrode. *J. Electrochem. Soc.* **2004**, *151*, A1517–A1529.

30 Dargaville, S.; Farrell, T. Predicting active material utilization in $LiFePO_4$ electrodes using a multiscale mathematical model. *J. Electrochem. Soc.* **2010**, *157*, A830–A840.

31 Chen, G.; Song, X.; Richardson, T. Electron microscopy study of the $LiFePO_4$ to $FePO_4$ phase transition. *Electrochem. Solid State Lett.* **2006**, *9*, A295–A298.

32 Ramana, C. V.; Mauger, A.; Gendron, F.; Julien, C. M.; Zaghib, K. Study of the Li-insertion/extraction process in $LiFePO_4/FePO_4$. *J. Power Sources* **2009**, *187*, 555–564.

33 Bazant, M. Z. *10.626 Electrochemical Energy Systems*; Massachusetts Institute of Technology, MIT OpenCourseWare, http://ocw.mit.edu; license, Creative Commons BY-NC-SA, 2011.

34 Burch, D.; Singh, G.; Ceder, G.; Bazant, M. Z. Phase-transformation wave dynamics $LiFePO_4$. *Solid State Phenom.* **2008**, *139*, 95–100.

35 Bazant, M. Z.; Kilic, M. S.; Storey, B.; Ajdari, A. Towards an understanding of nonlinear electrokinetics at large voltages in concentrated solutions. *Adv. Colloid Interface Sci.* **2009**, *152*, 48–88.

36 Kuznetsov, A. M.; Ulstrup, J. *Electron Transfer in Chemistry and Biology: An Introduction to the Theory*; Wiley: Chichester, U.K., 1999.

37 Sekimoto, K. *Stochastic Energetics*; Springer: Berlin, 2010.

38 Groot, S. R. D.; Mazur, P. *Non-equilibrium Thermodynamics*; Interscience Publishers, Inc.: New York, 1962.

39 Balluffi, R. W.; Allen, S. M.; Carter, W. C. *Kinetics of Materials*; Wiley: Hoboken, NJ, 2005.

40 Prigogine, I.; Defay, R. *Chemical Thermodynamics*; John Wiley and Sons: New York, 1954.

41 Kilic, M. S.; Bazant, M. Z.; Ajdari, A. Steric effects on the dynamics of electrolytes at large applied voltages: II Modified Nernst-Planck equations. *Phys. Rev. E* **2007**, *75*, No. 021503.

42 Han, B.; der Ven, A. V.; Morgan, D.; Ceder, G. Electrochemical modeling of intercalation processes with phase field models. *Electrochim. Acta* **2004**, *49*, 4691–4699.

43 Singh, G. K.; Bazant, M. Z.; Ceder, G. Anisotropic surface reaction limited phase transformation dynamics in $LiFePO_4$. *ArXiv* **2007**, No. arXiv:0707.1858v1.

44 Beard, D. A.; Qian, H. Relationship between thermodynamic driving force and one-way fluxes in reversible processes. *PLoS ONE* **2007**, *2*, No. e144.

45 Bard, A. J.; Faulkner, L. R. *Electrochemical Methods*; J. Wiley & Sons, Inc.: New York, 2001.

46 Kulikovsky, A. A. *Analytical Modelling of Fuel Cells*; Elsevier: New York, 2010.

47 Eikerling, M.; Kornyshev, A. A. Modelling the performance of the cathode catalyst layer of polymer electrolyte fuel cells. *J. Electroanal. Chem.* **1998**, *453*, 89–106.

48 Ioselevich, A. S.; Kornyshev, A. A. Phenomenological theory of solid oxide fuel cell anode. *Fuel Cells* **2001**, *1*, 40–65.

49 Lai, W.; Ciucci, F. Thermodynamics and kinetics of phase transformation in intercalation battery electrodes - phenomenological modeling. *Electrochim. Acta* **2010**, *56*, 531–542.

50 Lai, W.; Ciucci, F. Mathematical modeling of porous battery electrodes - Revisit of Newman's model. *Electrochim. Acta* **2011**, *56*, 4369–4377.

51 Lai, W. Electrochemical modeling of single particle intercalation battery materials with different thermodynamics. *J. Power Sources* **2011**, *196*, 6534–6553.

52 Marcus, R. A. On the theory of oxidation-reduction reactions involving electron transfer. I. *J. Chem .Phys.* **1956**, *24*, 966–978.

53 Marcus, R. A. . On the theory of electron-transfer reactions. VI. unified treatment for homogeneous and electrode reactions. *J. Chem .Phys.* **1965**, *43*, 679–701.

54 Marcus, R. A. Electron transfer reactions in chemistry. Theory and experiment. *Rev. Mod. Phys.* **1993**, *65*, 599–610.

55 Gelfand, I. M.; Fomin, S. V. *Calculus of Variations*; Dover: New York, 2000.

56 Cahn, J. W.; Hilliard, J. W. Free energy of a non-uniform system: I. Interfacial energy. *J. Chem. Phys.* **1958**, *28*, 258–267.

57 van der Waals, J. D. The thermodynamic theory of capillarity under the hypothesis of a continuous variation of density. *Verh. K. Akad. Wet., Afd. Natuurkd., Amsterdam (Sect. 1)* **1893**, *1*, 8. Translation by Rowlinson, J. S. *J. Stat. Phys.* **1979**, *20*, 197–244.

58 Nauman, E. B.; Heb, D. Q. Nonlinear diffusion and phase separation. *Chem. Eng. Sci.* **2001**, *56*, 1999–2018.

59 Bazant, M. Z.; Storey, B. D.; Kornyshev, A. A. Double layer in ionic liquids: Overscreening versus crowding. *Phys. Rev. Lett.* **2011**, *106*, No. 046102.

60 Bazant, M. Z.; Bažant, Z. P. Theory of sorption hysteresis in nanoporous solids: II. Molecular condensation. *J. Mech. Phys. Solids* **2012**, *60*, 1660–1675.

61 Murau, P.; Singer, B. The understanding and elimination of some suspension instabilities in an electrophoretic display. *J. Appl. Phys.* **1978**, *49*, 4820–4829.

62 Garcia, R. E.; Bishop, C. M.; Carter, W. C. Thermodynamically consistent variational principles with applications to electrically and magnetically active systems. *Acta Mater.* **2004**, *52*, 11–21.

63 Guyer, J. E.; Boettinger, W. J.; Warren, J. A.; McFadden, G. B. Phase field modeling of electrochemistry I: Equilibrium. *Phys. Rev. E* **2004**, *69*, No. 021603.

64 Guyer, J. E.; Boettinger, W. J.; Warren, J. A.; McFadden, G. B. Phase field modeling of electrochemistry II: Kinetics. *Phys. Rev. E* **2004**, *69*, No. 021604.

65 Tang, M.; Belak, J. F.; Dorr, M. R. Anisotropic phase boundary morphology in nanoscale olivine electrode particles. *J. Phys. Chem. C* **2011**, *115*, 4922–4926.

66 Liang, L.; Qi, Y.; Xue, F.; Bhattacharya, S.; Harris, S. J.; Chen, L.-Q. Nonlinear phase-field model for electrode-electrolyte interface evolution. *Phys. Rev. E* **2012**, *86*, No. 051609.

67 Samin, S.; Tsori, Y. Vapor-liquid equilibrium in electric field gradients. *J. Phys. Chem. B* **2011**, *115*, 75–83.

68 Storey, B. D.; Bazant, M. Z. Effects of electrostatic correlations on electrokinetic phenomena. *Phys. Rev. E* **2012**, *86*, No. 056303.

69 Santangelo, C. D. Computing counterion densities at intermediate coupling. *Phys. Rev. E* **2006**, *73*, No. 041512.

70 Hatlo, M. M.; Lue, L. Electrostatic interactions of charged bodies from the weak to the strong coupling regime. *Europhys. Lett.* **2010**, *89*, No. 25002.

71 Gregersen, M. M.; Okkels, F.; Bazant, M. Z.; Bruus, H. Topology and shape optimization of induced-charge electro-osmotic micropumps. *New J. Phys.* **2009**, *11*, 075016.

72 Biesheuvel, P. M.; van Soestbergen, M.; Bazant, M. Z. Imposed currents in galvanic cells. *Electrochim. Acta* **2009**, *54*, 4857–4871.

73 Biesheuvel, P.; Fu, Y.; Bazant, M. Diffuse charge and Faradaic reactions in porous electrodes. *Phys. Rev. E* **2011**, *83*, No. 061507.

74 Aziz, M. J.; Sabin, P. C.; Lu, G. Q. The activation strain tensor: Nonhydrostatic stress effects on crystal growth kinetics. *Phys. Rev. B* **1991**, *41*, 9812–9816.

75 Raistrick, I. D.; Mark, A. J.; Huggins, R. A. Thermodynamics and kinetics of the electrochemical insertion of lithium into tungsten bronzes. *Solid State Ionics* **1981**, *5*, 351–354.

76 Smith, K. C.; Mukherjee, P. P.; Fisher, T. S. Columnar order in jammed $LiFePO_4$ cathodes: Ion transport catastrophe and its mitigation. *Phys. Chem. Chem. Phys.* **2012**, *14*, 7040–7050.

77 Bai, P.; Tian, G. Statistical kinetics of phase-transforming nanoparticles in $LiFePO_4$ porous electrodes. *Electrochim. Acta* **2013**, *89*, 644–651.

78 Laughlin, R. B.; Pine, D.; Schmalian, J.; Stojkovic, B. P.; Wolynes, P. The middle way. *Proc. Natl. Acad. Sci. U.S.A.* **2000**, *97*, 32–37.